nature communications

Article

https://doi.org/10.1038/s41467-025-61191-5

The N-degron pathway governs autophagy to promote thermotolerance in *Arabidopsis*

Received: 8 November 2024

Accepted: 13 June 2025

Published online: 01 July 2025

Check for updates

Seu Ha Kim[1], Jun Seok Park[1], Myoung-Hoon Lee[1], Joongyu Seo[2], Jaekwan Kim[3], Woo Seok Yang[1], Jihye Park[1], Kwangmin Yoo[2], Jungmin Choi[2], Jong-Bok Seo[3], Hyun Kyu Song[1] & Ohkmae K. Park[1]

Autophagy is a vital process that enables plants to adapt to various environmental changes. During heat stress (HS), misfolded and denatured proteins accumulate in cells, necessitating autophagy for their removal. Here, we show that a core autophagy component ATG8a is targeted for degradation via the Arg/N-degron pathway. *ATG8a* is expressed as two alternatively spliced transcripts encoding ATG8a isoforms, namely ATG8a(S) and ATG8a(L), with distinct N-termini. While ATG8a(S) remains stable, ATG8a(L) is N-terminally processed to expose the Arg/N-degron, leading to its degradation. Ubiquitin protein ligase E3 component N-recognin 7 (UBR7), identified as an N-recognin, is responsible for ubiquitination and proteasomal degradation of ATG8a(L). Notably, *ATG8a*(*S*) and *ATG8a*(*L*) show dynamic expression patterns, fluctuating ATG8a levels during the HS and recovery periods. Our findings highlight the crucial role of ATG8a turnover in conferring thermotolerance, which is governed by Arg/N-degron-mediated regulation. Understanding the molecular basis of ATG8a stability will provide valuable insights into plant resilience to HS under changing climatic conditions.

N-degron pathways are proteolytic systems that control the half-life of proteins based on the identity of N-terminal residues[1–4]. Nascent proteins are synthesized with the N-terminal Met but can be post-translationally processed to expose new N-terminal residues that serve as degradation signals, termed N-degrons, making proteins short-lived in vivo. The N-terminal residues are recognized by E3 ubiquitin (Ub) ligase N-recognins that lead to polyubiquitination and proteasomal degradation via the Ub-proteasome system (UPS). In eukaryotes, five N-degron pathways have been defined as: the Arg/N-degron[2,3], Ac/N-degron[5,6], Pro/N-degron[7,8], formyl-Met/N-degron[9], and Gly/N-degron[10] pathways. The Arg/N-degron pathway is divided into two branches, in which type I basic (Arg, Lys, His, Cys, Asp, Glu) and type II bulky hydrophobic (Phe, Tyr, Trp, Leu, Ile) N-terminal residues are recognized by the UBR box and ClpS-like domain of N-recognins, respectively[11,12]. Arg/N-degrons often arise via enzymatic cascade reactions.

Yeast has a single Arg/N-recognin, Ub protein ligase E3 component N-recognin 1 (UBR1), but the mammalian genome encodes seven UBR box-containing proteins (UBR1-UBR7), of which UBR1, UBR2, UBR4, and UBR5 have been shown to function as N-recognins[2,3,13]. In plants, two N-recognins, PROTEOLYSIS 1 (PRT1) and PRT6, have been identified[14,15]. PRT6 contains the UBR box recognizing the type I N-terminal Arg and exhibits high sequence similarity to UBR[16]. PRT1 recognizes type II residues (Phe, Tyr, Trp) via the ZZ domain, which is different from the ClpS-like domain in UBRs[17]. A recent study has reported that BIG works together with PRT6 and PRT1 in the N-degron pathway, likely acting as an N-recognin[18]. Unlike plants, in yeast and animals, type I and II recognition sites reside within the same UBR protein. N-degron pathways target diverse substrates and regulate a wide array of biological processes[3,4,11,19]. In plants, substantial progress has been made in the study of the Arg/N-degron pathway, which functions as an O_2 and NO sensor in response to hypoxia under conditions of waterlogging or submergence[19–22].

Macroautophagy (hereafter autophagy) is a highly conserved cellular process in eukaryotes that engulfs cellular components into

[1]Department of Life Sciences, Korea University, Seoul, Korea. [2]Department of Biomedical Sciences, Korea University College of Medicine, Seoul, Korea. [3]Korea Basic Science Institute, Seoul Center, Seoul, Korea. e-mail: omkim@korea.ac.kr

double membrane-bound autophagosomes and delivers them to the vacuole or lysosome for degradation and recycling[23,24]. Autophagy was initially regarded as a bulk degradation process induced under nutrient deprivation and stress conditions, but it has become clear that it functions to maintain cellular homeostasis by selectively degrading specific targets, such as protein aggregates and damaged organelles, in a process termed selective autophagy[25]. In animal systems, the autophagic adaptor p62 acts as an N-recognin mediating crosstalk between UPS and autophagy[26–29]. Autophagosome formation is an essential part of autophagy and requires core autophagy machinery composed of autophagy-related (ATG) proteins. Molecular and genetic analyses of autophagy-defective *atg* mutants indicate that autophagy plays important roles in development and abiotic and biotic stress responses[30].

Most ATG proteins assemble into complexes and are recruited to the phagophore assembly site (PAS) to mediate a series of autophagic events[24,31–34]. In addition to its role in phagophore expansion, ATG8 is essential for cargo selection in selective autophagy through its interaction with cargo receptors such as Neighbor of Brca1 (NBR1)[35]. In contrast to a single ATG8 in yeast, ATG8 is diversified in higher eukaryotes. For example, *Arabidopsis* has nine ATG8 isoforms (ATG8a-i). While the reason of ATG8 diversity remains elusive, ATG8 variants may have specificity for cargo receptors to target distinct cargos in selective autophagy[36]. Despite substantial studies into autophagosome biogenesis and its components, the dynamic features of autophagy are not fully understood. Here we report that the Arg/N-degron pathway regulates temporal ATG8a turnover during heat stress (HS) responses, which is a crucial process ensuring plant survival in fluctuating thermal environments.

Results

ATG8a is regulated by the Arg/N-degron pathway

To explore the role of ATG8, we expressed two *Arabidopsis* ATG8 isoforms, ATG8a and ATG8e, fused with either an N-terminal MYC tag (MYC-ATG8a/8e) or a C-terminal hemagglutinin (HA) tag (ATG8a/8e-HA) in wild-type Col-0 protoplasts. Since newly synthesized ATG8 proteins are known to undergo immediate cleavage by ATG4 protease to expose the C-terminal Gly residue[34,37,38], we introduced mutations to prevent this cleavage and loss of the C-terminal tag. Specifically, we substituted the C-terminal residues $FGS^{131–133}$ with AAA in ATG8a and $FG^{117–118}$ with AA in ATG8e to generate non-cleavable (NC) mutants, which were then used for C-terminal fusion constructs. Expression analysis revealed that, unlike ATG8e, ATG8a protein levels were unexpectedly low regardless of the type and position of affinity tags, despite comparable transcript levels between *ATG8a* and *ATG8e* (Fig. 1a). This intriguing observation led us to suspect that ATG8a might be degraded by the UPS. To test this, we monitored ATG8a expression in the presence of the proteasome inhibitor MG132. Immunoblotting with antibodies against the HA tag and ATG8a revealed that MG132 treatment increases the protein levels of ATG8a (Fig. 1b). However, MYC-ATG8a proteins remained barely detectable by the anti-MYC antibody, suggesting that the N-terminal part of ATG8a may be lost. In contrast, ATG8e expression was unaffected by MG132 treatment. Untagged ATG8a proteins were also stabilized by MG132 treatment (Fig. 1c). Therefore, affinity tags are unlikely to interfere with ATG8a expression. The specificity of the anti-ATG8a antibody for ATG8a was validated by immunoblot analysis using purified recombinant proteins of ATG8 isoforms (ATG8a-i) (Supplementary Fig. 1a), excluding the possibility of cross-reactivity with other ATG8 isoforms in *Arabidopsis*. These immunoblotting data suggest that ATG8a undergoes 26S proteasome-dependent degradation, potentially involving the truncation of its N-terminal part. The degradation patterns of ATG8a were similar in protoplasts from wild-type plants grown under both long-day and short-day conditions, indicating that ATG8a stability is not influenced by photoperiods (Supplementary Fig. 1b).

Alignment of ATG8a and ATG8e sequences revealed that ATG8a has 14 additional amino acids at the N-terminus compared to ATG8e, suggesting that these extra residues might contribute to the stability difference between ATG8a and ATG8e (Fig. 1d). To investigate this, we expressed an ATG8a variant with the N-terminal 14 residues deleted ($ATG8a^{\Delta 14}$) and found that this deletion stabilizes ATG8a (Fig. 1e). This N-terminus-dependent ATG8a degradation led to the plausible assumption that ATG8a contains an N-degron and is regulated by the N-degron pathway. Notably, the N-terminal sequence of ATG8a features characteristics of an Arg/N-degron, with Arg at position 13 followed by a hydrophobic residue Ile at position 14 (Fig. 1d)[39]. Indeed, Arg 13 to Ala mutation stabilized $ATG8a^{R13A}$, while $MYC\text{-}ATG8a^{R13A}$ remained barely detectable by the anti-MYC antibody (Fig. 1f). These results suggest that ATG8a exposes Arg at the N-terminus as a primary destabilizing residue after cleavage before R^{13} and undergoes Arg/N-degron-mediated degradation.

Upon autophagy activation, ATG8 undergoes lipidation, resulting in the formation of a phosphatidylethanolamine (PE)-conjugate at the C-terminal Gly (G^{132} in ATG8a; Fig. 1d). ATG8-PE is then recruited to autophagosomes and delivered to the vacuole, where it is degraded[34,37,38]. Thus, we investigated whether ATG8a is degraded via the vacuolar pathway by assessing ATG8a stability in the presence of concanamycin A (ConA), a known inhibitor of vacuolar degradation. In contrast to MG132, ConA treatment did not affect the stabilization of ATG8a (Supplementary Fig. 1c), reinforcing the notion that ATG8a degradation occurs via the Arg/N-degron pathway. Moreover, expression of NC forms of ATG8a and ATG8e, relative to the tonoplast K^+ channel two-pore K^+ 1 (TPK1)[40], revealed that they are not delivered to the vacuole (Supplementary Fig. 1d), further reducing the possibility of vacuolar degradation of ATG8aNC/8eNC.

ATG8a is N-terminally cleaved to expose the Arg/N-degron

To investigate the N-terminal truncation of ATG8a, residues around R^{13} of MYC-ATG8a were mutated to determine whether these mutant proteins are detectable with an anti-MYC antibody (Fig. 2a). Unlike wild-type MYC-ATG8a, $MYC\text{-}ATG8a^{7A}$ with mutations in 7 residues (positions 10–16) around R^{13} was stably detected by the anti-MYC antibody (Fig. 2b). $MYC\text{-}ATG8a^{3A}$ with mutations in 3 residues (positions 10–12) before R^{13}, but not $MYC\text{-}ATG8a^{AVG}$ with $RIA^{13–15}$ to AVG substitutions, was also detected by the anti-MYC antibody, suggesting that residues before R^{13} are important for N-terminal cleavage of ATG8a (Fig. 2b). Separation of proteins on a 16.5% Tris-Tricine gel allowed for the detection of the cleaved MYC tag in MYC-ATG8a and $MYC\text{-}ATG8a^{AVG}$ (Fig. 2c). Further mutational analysis of three residues preceding R^{13} showed that two residues, T^{11} and N^{12}, are critical for N-terminal truncation of ATG8a (Fig. 2d). These findings align with earlier studies, which demonstrated that the residues N-terminal to the cleavage site in substrate proteins largely determine the specificity of proteolytic enzymes[41].

When ATG8a, fused with three MYC tags (3xMYC) at its N-terminus, was expressed in the presence of MG132, a noticeable reduction in the molecular size of ATG8a and $ATG8^{R13A}$ by ~5 kDa was observed (Fig. 2e). This size decrease corresponds to the removal of 3xMYC and N-terminal 12 residues. In contrast, $ATG8a^{3A}$ retained the MYC tag, further supporting the N-terminal processing in ATG8a. To verify that ATG8a exposes R^{13} at the N-terminus, we raised the anti-R^{13}-ATG8a antibody that specifically recognizes R^{13}-ATG8a using the peptide $RIAMAKSSFKI^{13–23}$. We also prepared R^{13}-ATG8a and A^{13}-ATG8a with an Arg 13 to Ala substitution using the LC3B-fusion technique, which produces proteins bearing desired N-terminal residues[16]. Immunoblot analysis using R^{13}-ATG8a and A^{13}-ATG8a and the peptide competition assay confirmed the antibody specificity for R^{13}-ATG8a (Supplementary Fig. 1e). As predicted, the anti-R^{13}-ATG8a antibody immunoblotted both untagged and tagged ATG8a stabilized by MG132 treatment, but not $ATG8a^{R13A}$ and $ATG8a^{3A}$ (Fig. 2f).

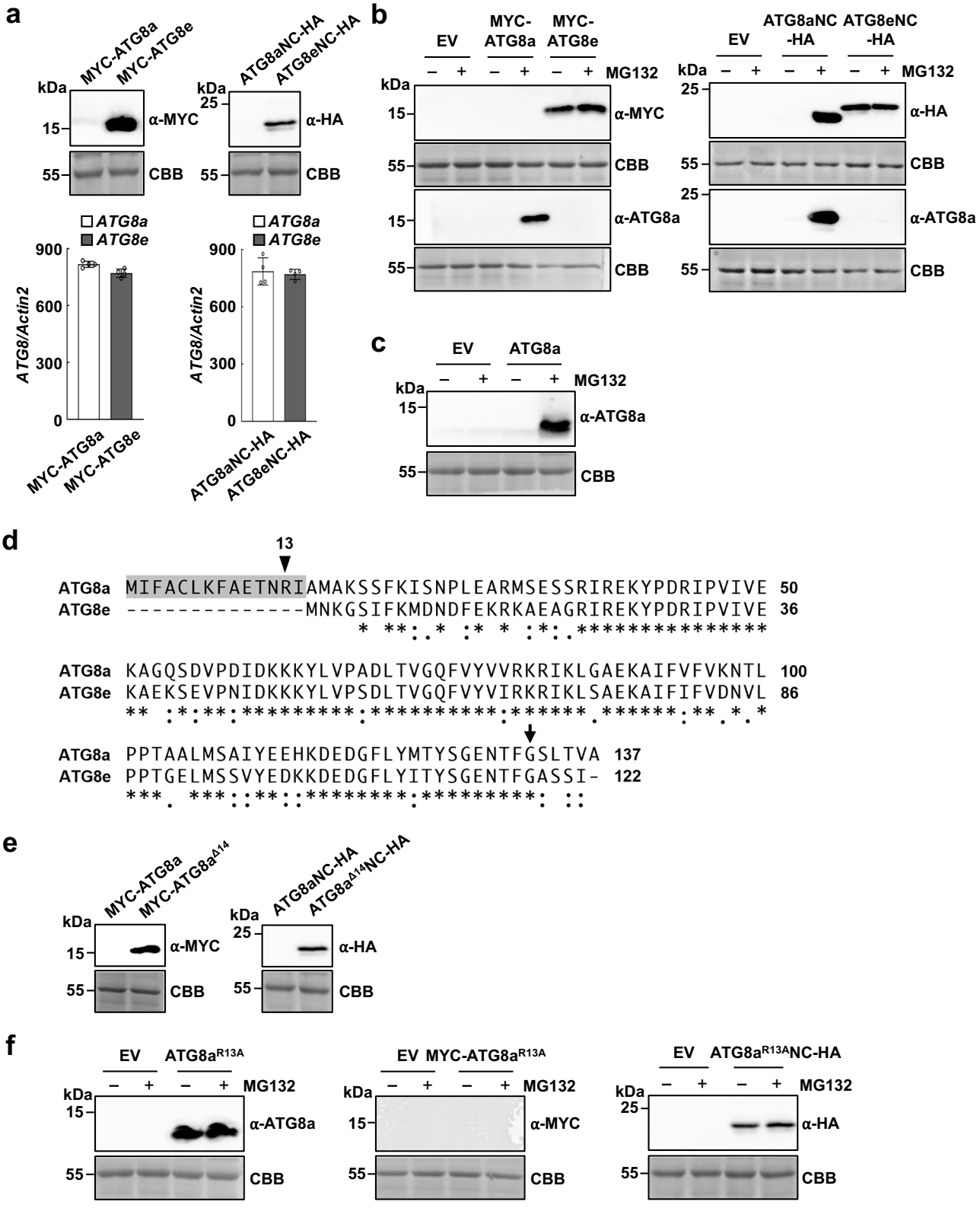

Next, we tested for ATG8a ubiquitination in an in vivo ubiquitination assay in protoplasts by co-expressing MYC-tagged Ub. Consistently, high-molecular-weight smears, indicative of polyubiquitination, were observed for ATG8a, but not for ATG8a$^{\Delta 14}$, ATG8^{R13A}, and ATG8a^{3A}, which were resistant to proteasomal degradation (Fig. 2g). Collectively, our results suggest that N-terminally truncated R^{13}-ATG8a is a target substrate of the Arg/N-degron pathway.

UBR7 functions as an N-recognin for ATG8a

Next, we sought to identify an N-recognin that targets ATG8a to proteasomal degradation via the Arg/N-degron pathway. *Arabidopsis* has three UBR box-containing proteins, PRT6, BIG[42], and AT4G23860[4]. AT4G23860, which shows considerable similarity to mammalian UBR7, is hereafter referred to as *Arabidopsis* UBR7 (Supplementary Fig. 2). UBR7 possesses a PHD domain, which has been previously shown to be responsible for E3 Ub ligase activity[43–45]. We examined whether ATG8a

Fig. 1 | ATG8a undergoes Arg/N-degron-mediated degradation. a ATG8a expression is barely detectable in Col-0 protoplasts. MYC-ATG8a/ATG8e and ATG8aNC/ATG8eNC-HA were expressed in Col-0 protoplasts. Protein (upper) and transcript (lower) levels were determined by immunoblotting and RT-qPCR, respectively. Data represent means ± SD ($n = 4$ biological replicates). **b**, **c** ATG8a either with (**b**) or without (**c**) affinity tags undergo 26S proteasome-dependent degradation. MYC-ATG8a/ATG8e, ATG8aNC/ATG8eNC-HA, and untagged ATG8a were expressed in Col-0 protoplasts, followed by treatments with cycloheximide (100 μM) and MG132 (10 μM) for 3 h. EV, empty vector. **d** Sequence alignment of ATG8a and ATG8e shows that ATG8a has 14 additional amino acids at the N-terminus compared to ATG8e. Sequences were aligned using Clustal Omega online (https://www.ebi.ac.uk/Tools/msa/clustalo/). The N-terminal 14 residues are shaded, and the putative N-degron residue R^{13} is indicated by an arrowhead in ATG8a. The Gly residue exposed at the C-terminus after C-terminal cleavage and conjugated to PE is indicated by an arrow. Consensus symbols are as follows: asterisks indicate identical residues; colons and periods indicate conserved and semiconserved substitutions, respectively. **e** Deletion of N-terminal 14 residues stabilizes ATG8a. MYC-ATG8a/ATG8a$^{\Delta 14}$ and ATG8aNC/ATG8a$^{\Delta 14}$NC-HA were expressed in Col-0 protoplasts. **f** R^{13}A mutation stabilizes ATG8a. ATG8a^{R13A} without affinity tags, MYC-ATG8a^{R13A}, and ATG8a^{R13A}NC-HA were expressed in Col-0 protoplasts, followed by treatments with cycloheximide (100 μM) and MG132 (10 μM) for 3 h. EV, empty vector. ATG8a proteins were analyzed by immunoblotting with respective antibodies (**a**–**c**, **e**, **f**), and Coomassie brilliant blue (CBB) staining served as a loading control (**a**–**c**, **e**, **f**). Three independent experiments were repeated with similar results (**a**–**c**, **e**, **f**).

stability is regulated by PRT6, BIG, or UBR7. In transient expression assays, ATG8aNC-HA did not accumulate without MG132 treatment in protoplasts of *prt6-1* and *big-3* knockout mutants, similar to wild-type protoplasts (Fig. 3a). Since PRT6 is a known N-recognin, an artificial R-GUS substrate with the N-terminal Arg was generated through the Ub fusion technique[1], and its degradation was tested in *prt6-1* protoplasts, as previously reported[14]. R-GUS proteins, but not M-GUS, underwent proteasomal degradation in wild-type protoplasts, while both R- and M-GUS accumulated in *prt6-1* (Supplementary Fig. 3a). These results imply that the N-terminal Arg of N-degron substrates is required but not sufficient for specific binding to N-recognins. Notably, ATG8aNC-HA levels were elevated in *ubr7* protoplasts regardless of MG132 treatment (Fig. 3b, Supplementary Fig. 3b–d). Similarly, R^{13}-ATG8a, generated through the Ub fusion technique, was degraded in wild-type protoplasts but stabilized in *ubr7*, unlike A^{13}-ATG8a, which was stably expressed (Fig. 3c). These results suggest that UBR7 is the cognate N-recognin for R^{13}-ATG8a.

To assess the interaction between ATG8a and UBR7, bimolecular fluorescence complementation (BiFC) assays were conducted by co-expressing UBR7 or the UBR box domain of UBR7 fused with the N-terminal half of green fluorescent protein (GFP^N) and ATG8aNC, ATG8a^{R13A}NC, and ATG8a^{3A}NC fused with the C-terminal half of GFP (GFP^C) under the CaMV 35S promoter in protoplasts (Supplementary Fig. 3e). GFP signals were detected only in protoplasts co-expressing UBR7/UBR box and ATG8aNC, while both UBR7 and UBR box domain showed no fluorescent signals with ATG8a^{R13A}NC and ATG8a^{3A}NC (Fig. 3d, Supplementary Fig. 3f). It was noted that UBR7 is expressed and interacts with ATG8aNC only in the nucleus, as overlapped with the nuclear 4′,6-diamidino-2-phenylindole (DAPI) signal, although ATG8aNC is localized in both the cytoplasm and nucleus (Fig. 3d, Supplementary Fig. 4). Their interaction was further evaluated by a co-immunoprecipitation assay in protoplasts. Consistently, UBR7 co-immunoprecipitated with ATG8aNC, but not with ATG8a^{R13A}NC and ATG8a^{3A}NC (Fig. 3e). Moreover, it was confirmed that UBR7 binds specifically to the N-terminal Arg of ATG8a using R^{13}-ATG8a and A^{13}-ATG8a proteins prepared by the LC3B-fusion technique[16]. An in vitro pull-down assay clearly showed a specific interaction between MYC-UBR7 and R^{13}-ATG8a (Fig. 3f). Since mammalian UBR7 was previously shown to have E3 Ub ligase activity[43], we investigated whether *Arabidopsis* UBR7 functions as an E3 Ub ligase N-recognin. MYC-UBR7 and its mutant MYC-mUBR7 with $H^{157}S$ and $H^{160}S$ substitutions[43] were incubated with R^{13}-ATG8a and A^{13}-ATG8a in an in vitro ubiquitination assay. The results indicated that UBR7, but not mUBR7, can polyubiquitinate R^{13}-ATG8a but not A^{13}-ATG8a (Fig. 3g). In an in vivo ubiquitination assay, ATG8a ubiquitination was not observed in *ubr7* protoplasts but was restored by transient expression of UBR7 (Supplementary Fig. 5). Together, these results demonstrate that UBR7, acting as an N-recognin, recognizes and polyubiquitinates ATG8a with Arg exposed at its N-terminus.

These findings suggest that ATG8a degradation may be linked to its nuclear transport. We then investigated whether ATG8a-specific N-terminal sequence serves as a nuclear localization signal. For this, GFP was fused with the N-terminal 15 amino acids of ATG8a and expressed in protoplasts (Supplementary Fig. 6). GFP signals were detected in the cytoplasm regardless of the presence or absence of the N-terminal peptide, suggesting that this sequence alone does not determine the nuclear transport of ATG8a. While other yet unidentified regulatory mechanisms may facilitate ATG8a nuclear import, previous studies in yeast have shown that cytoplasmic proteins are transported to the nucleus via chaperones, followed by ubiquitination and degradation, highlighting a role for the nucleus in quality control of cytoplasmic proteins[46,47].

ATG8a is expressed as splice variants *ATG8a*(*S*) and *ATG8a*(*L*)

While investigating the biological significance of ATG8a regulation by the Arg/N-degron pathway, we had an intriguing finding in the genomic structure that *ATG8a* undergoes alternative splicing (AS) and is expressed as two splice variants, AT4G21980.1 and AT4G21980.2 (Fig. 4a). AT4G21980.2 is an intron retention (IR) variant that encodes ATG8a with an additional 15 amino acids at the N-terminus, bearing the N-degron; AT4G21980.1 and AT4G21980.2 are hereafter designated as *ATG8a*(*S*) and *ATG8a*(*L*), respectively. Since ATG8a(L) expression leads to the elimination of ATG8a proteins, differential generation of these splice variants may be a mechanism to modulate ATG8a protein levels.

ATG8a(L) expression leads to N-degron-mediated ATG8a degradation during thermorecovery

Considering that autophagy is critical for plant adaptation to the environment, we examined whether Arg/N-degron-mediated ATG8a(L) regulation contributes to stress responses. For this, we analyzed the expression patterns of ATG8a(S) and ATG8a(L) in *Arabidopsis* Col-0 plants during stress responses with three criteria: (1) induction of *ATG8a*(*L*) expression, (2) concurrent decrease in ATG8a protein levels, and (3) restoration of reduced ATG8a levels with MG132 treatment. Given that autophagy is important for clearing protein aggregates, we investigated its relevance to endoplasmic reticulum (ER) stress caused by the accumulation of unfolded and misfolded proteins. The expression of *ATG8a*(*S*) and *ATG8a*(*L*) was monitored in plants after treatments with dithiothreitol (DTT) and tunicamycin (TM), two common ER stress inducers[48]. While the transcript level of *ATG8a*(*L*) was significantly lower than that of *ATG8a*(*S*), both *ATG8a*(*S*) and *ATG8a*(*L*) showed increased expression in response to DTT and TM treatments (Supplementary Fig. 7a, b). In contrast, ATG8a protein levels decreased after peaking at 12 h and 48 h, respectively, which was not significantly affected by MG132 treatment (Supplementary Fig. 7c, d). These results suggest that ATG8a(L) degradation via the N-degron pathway is not implicated in ER stress responses.

HS is a detrimental abiotic stress that also leads to the accumulation of heat-denatured protein aggregates. Given the important role of autophagy in thermotolerance and HS recovery[49,50], we analyzed the expression of *ATG8a*(*S*) and *ATG8a*(*L*) during HS and recovery (Fig. 4b). *ATG8a*(*S*) was highly expressed in plants exposed to high temperature

https://doi.org/10.1038/s41467-025-61191-5

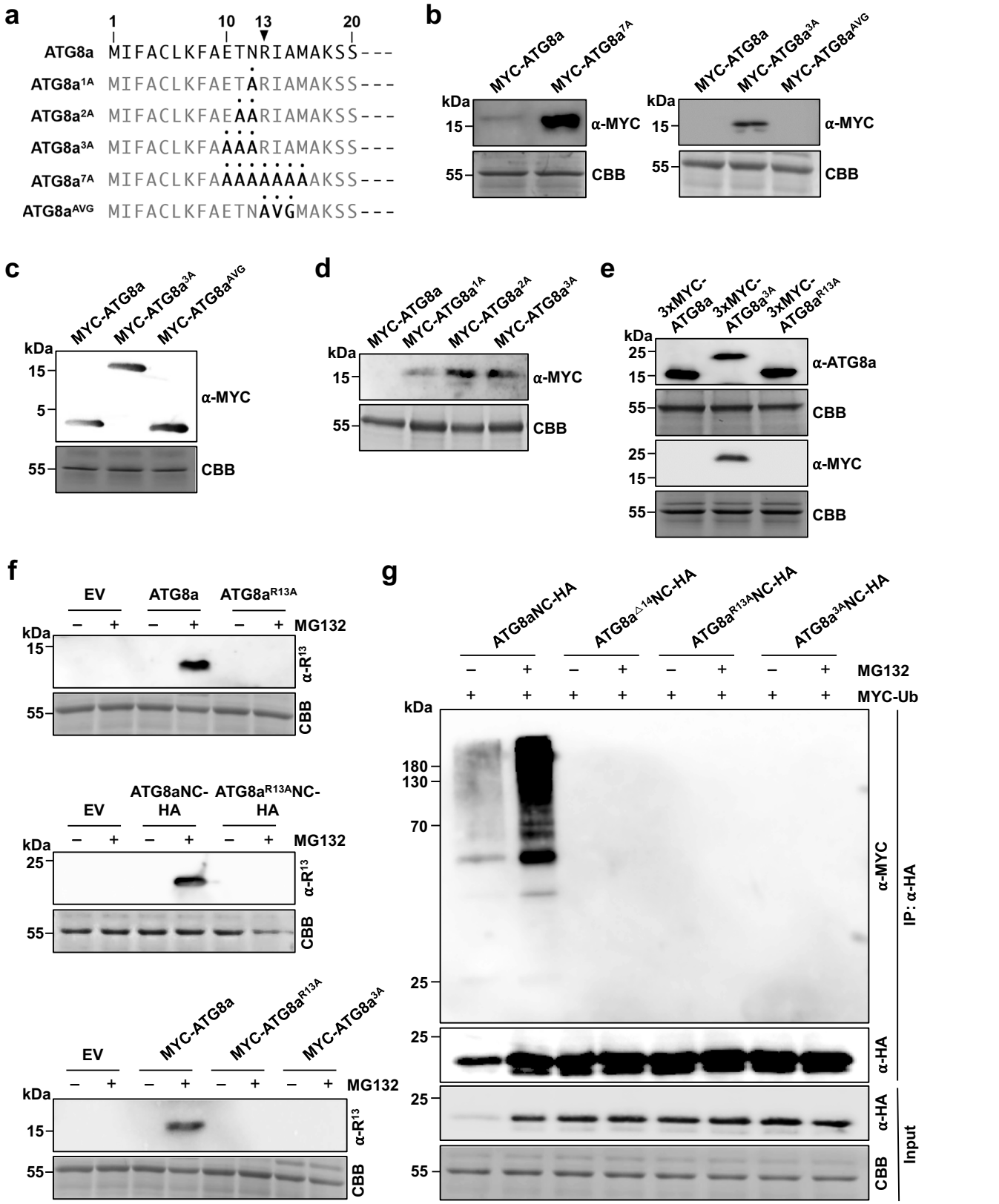

(42 °C) but decreased during HS recovery. In contrast, *ATG8a*(*L*) showed rapid induction after release from HS (Fig. 4b, inset), but its abundance was still three-fold less than that of *ATG8a*(*S*). We then determined the protein levels of ATG8a. ATG8a proteins accumulated under HS but largely decreased after HS (Fig. 4c). ATG8a proteins were barely detected in *atg8a* mutant (Fig. 4c), further verifying the specificity of the anti-ATG8a antibody. To investigate whether ATG8a undergoes turnover during HS recovery, we monitored its abundance in the presence of ConA or MG132 (Fig. 4d, e). Both inhibitors restored ATG8a levels, although ATG8a stabilized by ConA gradually declined over time. Notably, R^{13}-ATG8a accumulated only in the presence of MG132 during HS recovery, as revealed by immunoblotting with the

https://doi.org/10.1038/s41467-025-61191-5

Fig. 2 | ATG8a is N-terminally cleaved to expose the Arg/N-degron. a N-terminal sequences of ATG8a mutants with the indicated substitutions. **b** Mutations at residues preceding R^{13} stabilize ATG8a. MYC-tagged ATG8a, ATG8a^{7A}, ATG8a^{3A}, and ATG8a^{AVG} were expressed in Col-0 protoplasts. **c** ATG8a undergoes N-terminal cleavage. MYC-tagged ATG8a, ATG8a^{3A}, and ATG8a^{AVG} were expressed in Col-0 protoplasts. Proteins were separated on a 16.5% Tris-Tricine gel to visualize the cleaved MYC tag. **d** Mutations at T^{11} and N^{12} stabilize ATG8a. MYC-tagged ATG8a, ATG8a^{1A}, ATG8a^{2A}, and ATG8a^{3A} were expressed in Col-0 protoplasts. **e** ATG8a is N-terminally processed. ATG8a, ATG8a^{3A}, and ATG8a^{R13A} fused with 3 MYC tags (3xMYC) at the N-terminus were expressed in Col-0 protoplasts, followed by treatment with MG132 (10 μM) for 3 h. **f** ATG8a exposes R^{13} at the N-terminus. ATG8a, ATG8a^{R13A}, and ATG8a^{3A}, either with or without affinity tags, were expressed in Col-0 protoplasts, followed by treatments with cycloheximide (100 μM) and MG132 (10 μM) for 3 h. EV, empty vector; α-R^{13}, anti-R^{13}-ATG8a antibody. **g** In vivo ubiquitination assay for ATG8a polyubiquitination. ATG8aNC, ATG8a^{Δ14}NC, ATG8a^{R13A}NC, and ATG8a^{3A}NC fused with HA at the C-terminus were expressed together with MYC-Ub in Col-0 protoplasts, followed by treatment with MG132 (10 μM) for 3 h. Protein lysates were subjected to immunoprecipitation with the anti-HA antibody. Input shows 2% of the amount used in reactions. IP, immunoprecipitation. ATG8a proteins were analyzed by immunoblotting with respective antibodies (**b**–**g**), and Coomassie brilliant blue (CBB) staining served as a loading control (**b**–**g**). Three independent experiments were repeated with similar results (**b**–**g**).

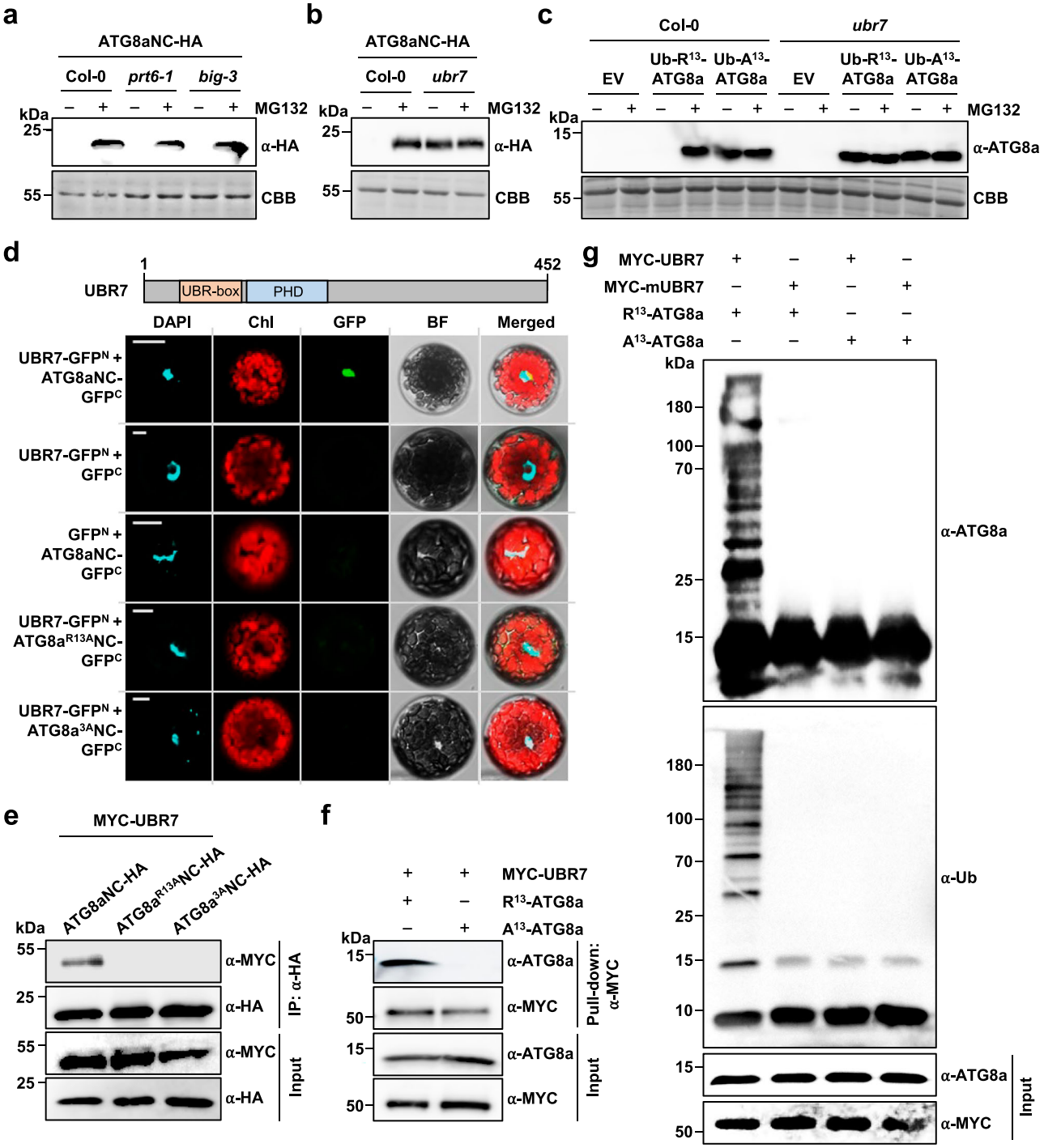

https://doi.org/10.1038/s41467-025-61191-5

Fig. 3 | UBR7 is an E3 Ub ligase N-recognin for ATG8a. a, **b** ATG8a expression is not altered in *prt6-1* and *big-3* (**a**) but is elevated in *ubr7* (**b**) mutants. ATG8aNC-HA was expressed in Col-0, *prt6-1*, *big-3*, and *ubr7* protoplasts, followed by treatments with cycloheximide (100 μM) and MG132 (10 μM) for 3 h. **c** R^{13}-ATG8a generated through the Ub fusion technique is degraded in wild-type but stabilized in *ubr7* mutant. Ub-R^{13}/A^{13}-ATG8a were expressed in Col-0 and *ubr7* protoplasts, followed by treatments with cycloheximide (100 μM) and MG132 (10 μM) for 3 h. EV empty vector. **d** BiFC assay for in vivo interaction between ATG8a and UBR7. The domain structure of *Arabidopsis* UBR7 is shown (top). GFP^N, GFP^C, and their fusions with UBR7, ATG8aNC, $ATG8a^{R13A}$NC, and $ATG8a^{3A}$NC were co-expressed in Col-0 protoplasts, followed by treatment with MG132 (10 μM) for 3 h. Reconstituted GFP fluorescence was visualized under a confocal microscope. DAPI staining indicates the location of nuclei. Chl chlorophyll, BF bright field. Bars, 10 μm. **e** In vivo co-immunoprecipitation assay for interaction between ATG8a and UBR7. Protein lysates were prepared from Col-0 protoplasts co-expressing MYC-UBR7 and ATG8aNC-HA, $ATG8a^{R13A}$NC-HA, or $ATG8a^{3A}$NC-HA, followed by treatment with MG132 (10 μM) for 3 h, and subjected to immunoprecipitation with the anti-HA antibody in the presence of MG132 (10 μM). Input shows 2% of the amount used in binding reactions. IP immunoprecipitation. **f** In vitro pull-down assay for interaction between ATG8a and UBR7. MYC-UBR7 was incubated with R^{13}- ATG8a or A^{13}-ATG8a and pulled down by incubation with the anti-MYC antibody and protein G agarose beads. Input shows 5% of the amount used in binding reactions. **g** In vitro ubiquitination assay for UBR7-mediated R^{13}-ATG8a polyubiquitination. MYC-UBR or MYC-mUBR7 was incubated with either R^{13}-ATG8a or A^{13}-ATG8a in the presence of Ub, human E1, and *Arabidopsis* E2 enzymes. Input shows 5% of the amount used in binding reactions. ATG8a and UBR7 proteins were analyzed by immunoblotting with respective antibodies (**a**–**c**, **e**–**g**), and Coomassie brilliant blue (CBB) staining served as a loading control (**a**–**c**). Three (**a**–**c**, **e**–**g**) and five (**d**) independent experiments were repeated with similar results.

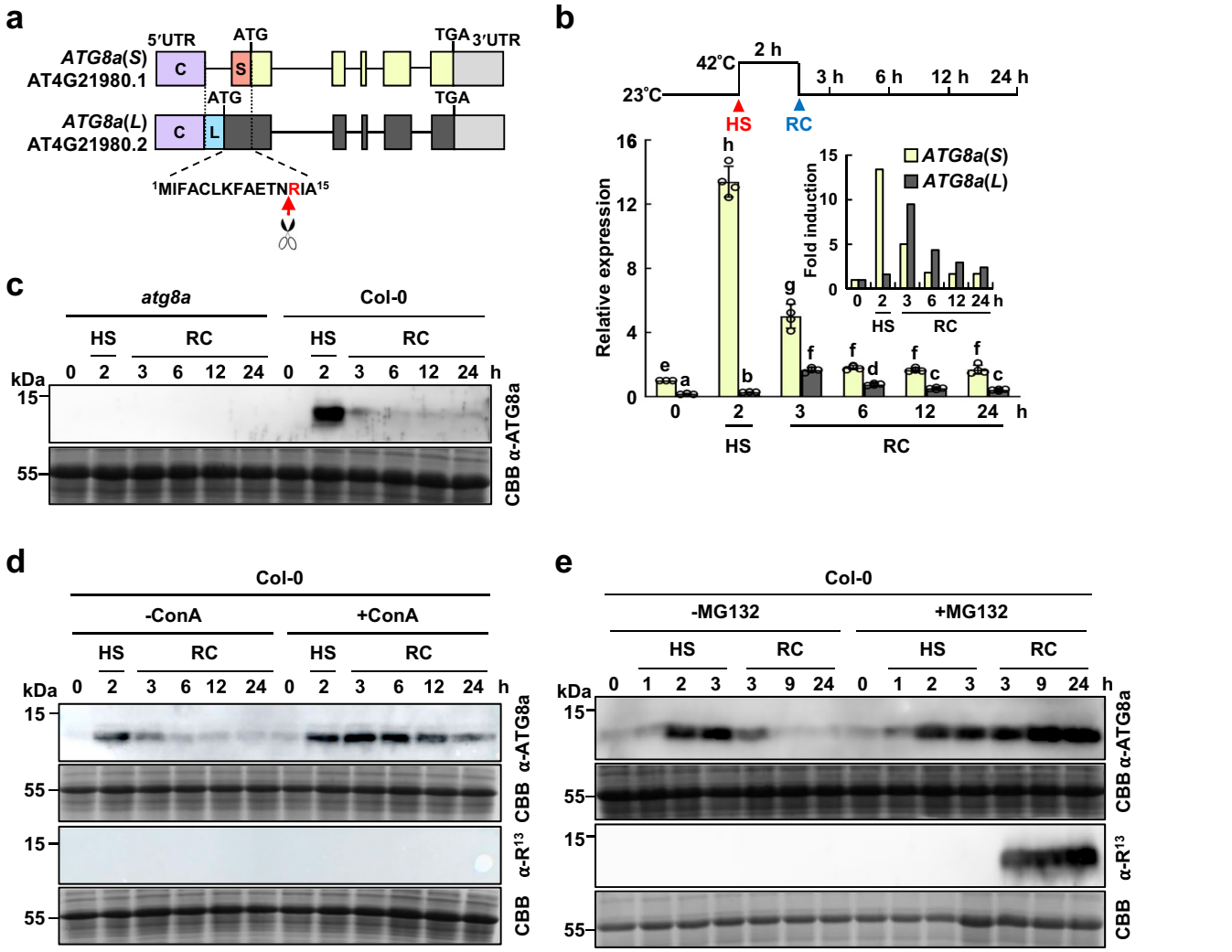

Fig. 4 | R^{13}-ATG8a is expressed and degraded during HS recovery. a Schematic diagram of ATG8a splice variants, *ATG8*(*S*) and *ATG8a*(*L*). Exons are indicated by yellow and dark gray (coding) and purple, red, blue, and light gray (UTRs) boxes. Introns are shown in lines. The additional N-terminal 15 residues in ATG8a(L) are shown at the bottom. **b** *ATG8*(*S*) and *ATG8a*(*L*) are differentially expressed during HS responses. *ATG8*(*S*) and *ATG8a*(*L*) expression were analyzed by RT-qPCR in Col-0 plants exposed to HS (42 °C) for 2 h and recovery (23 °C) for the indicated times. Data represent means ± SD ($n = 4$ biological replicates). Different letters indicate significant differences (Two-way ANOVA with Tukey's HSD test; $P < 0.05$). **c** ATG8a abundance changes during HS responses. ATG8a expression was monitored during HS and recovery in Col-0 and *atg8a* plants. **d** ATG8a undergoes vacuolar degradation during HS recovery. ATG8a expression was monitored in the presence or absence of ConA during HS and recovery in Col-0 plants. For ConA treatment, plants were infiltrated with ConA (1 μM) and incubated for 12 h prior to exposure to HS and recovery conditions. α-R^{13}, anti-R^{13}-ATG8a antibody. **e** ATG8a undergoes proteasomal degradation during HS recovery. ATG8a expression was monitored in the presence or absence of MG132 during HS and recovery in Col-0 plants. For MG132 treatment, plants were sprayed with MG132 (10 μM) and incubated for 1 h prior to exposure to HS and recovery conditions. α-R^{13}, anti-R^{13}-ATG8a antibody. ATG8a proteins were analyzed by immunoblotting with respective antibodies (**c**–**e**), and Coomassie brilliant blue (CBB) staining served as a loading control (**c**–**e**). Three independent experiments were repeated with similar results (**c**–**e**). HS heat stress (**c**–**e**); RC recovery (**c**–**e**).

https://doi.org/10.1038/s41467-025-61191-5

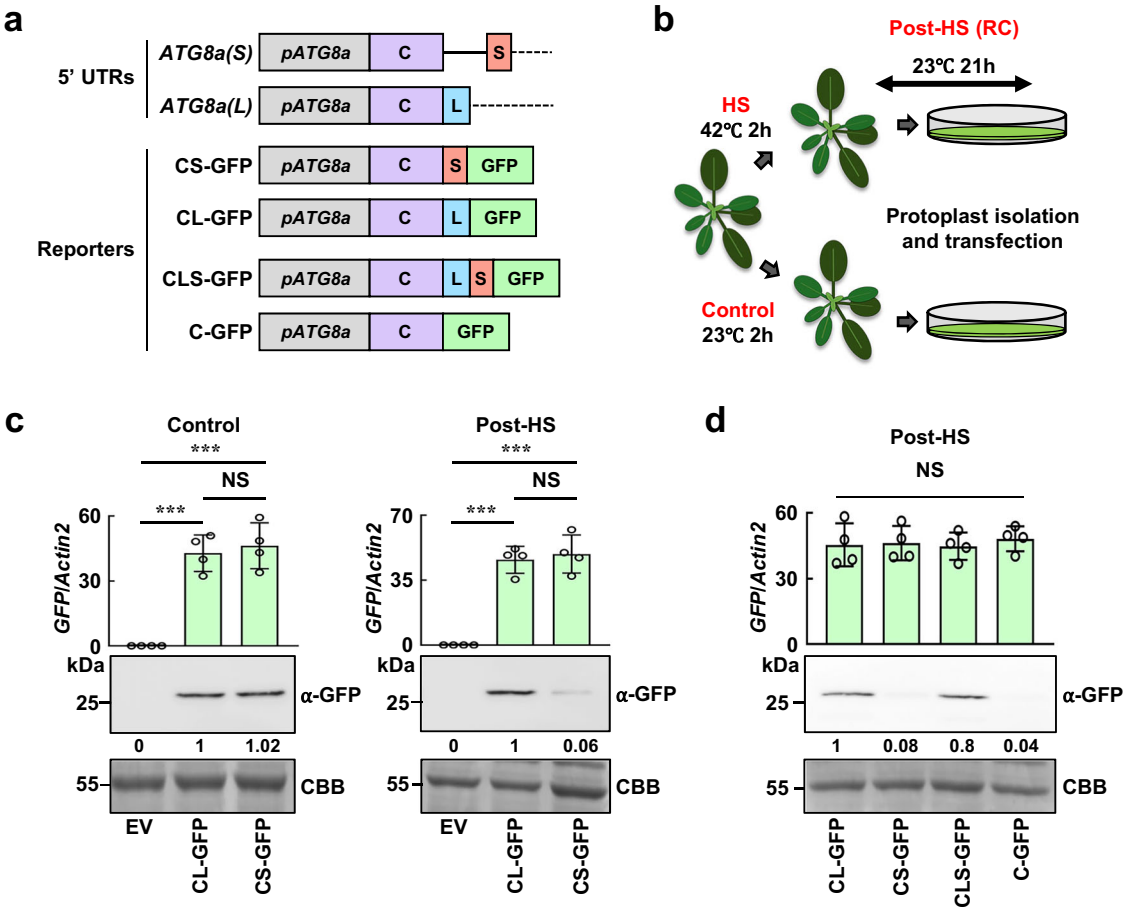

Fig. 5 | *ATG8a(L)* 5′ UTR enhances translation during HS recovery. a Schematic diagram of reporter constructs used for translational activity. 5′ UTRs of *ATG8(S)* and *ATG8a(L)* are shown, containing distinct sequences indicated as S and L, respectively, in addition to the common sequence C (top). The reporter constructs carry the native promoter *pATG8a* and different combinations of C, S, and L, fused to the *GFP* gene. **b** Scheme of HS treatment and post-HS (recovery) in protoplasts. Col-0 plants were exposed to HS at 42 °C for 2 h and subjected to reporter assays in protoplasts. Protoplast isolation and transfection were performed at 23 °C, and therefore this period was regarded as the post-HS. **c**, **d** *ATG8a(L)*-specific L sequence stimulates translation under post-HS. Control (no HS treatment) and post-HS protoplasts were transfected with reporter constructs carrying *ATG8a(L)* 5′ UTR (CL-GFP) and *ATG8a(S)* 5′ UTR (CS-GFP) (**c**) and different combinations of C, S, and L in 5′ UTRs (**d**). *GFP* transcript (top) and GFP protein (bottom) levels were determined by RT-qPCR and immunoblotting with the anti-GFP antibody, respectively. In RT-qPCR (top), *Actin2* was used as a control. Data represent means ± SD ($n = 4$ biological replicates). Asterisks indicate significant differences between EV and reporter constructs (Two-tailed Student's *t* test; ***$P < 0.001$; The *P* value are as follows. <0.0001, <0.0001, 0.6327 in Control (**c**); <0.0001, <0.0001, 0.6405 in Post-HS (**c**); One-way ANOVA with two-tailed Student's *t* test; $P = 0.9277$ (**d**)). In immunoblotting (bottom), Coomassie brilliant blue (CBB) staining served as a loading control. Relative intensities of GFP normalized to the loading control are shown as numerical values. HS heat stress, RC recovery, NS not significant, EV empty vector.

anti-R[13]-ATG8a antibody (Fig. 4e). These results suggest that AT8a(S), generated in response to HS, undergoes autophagic degradation, while ATG8a(L) accumulates and is degraded via the Arg/N-degron pathway during the HS recovery phase. Collectively, these findings demonstrate that ATG8a(S) and ATG8a(L) are major forms expressed during HS and recovery, respectively, with ATG8a(L) degradation contributing significantly to the reduction of ATG8a during the post-HS period.

ATG8a(L) 5′ UTR promotes translation of *ATG8a(L)* during thermorecovery

It was puzzling because *ATG8a(S)* transcripts accumulated at a much higher level than *ATG8a(L)*, making it difficult for ATG8a(L) to be expressed as the major form during HS recovery. Therefore, we reasoned that the production of ATG8a(S) and ATG8a(L) may be regulated by an additional post-transcriptional mechanism. Of note, *ATG8a(S)* and *ATG8a(L)* have distinct 5′ untranslated regions (UTRs), in which the 5′ part is common (designated as C) and the 3′ part contains sequences specific to each (designated as S and L, respectively) (Figs. 4a and 5a).

To examine the translational activity of 5′ UTRs of *ATG8a(S)* and *ATG8a(L)*, we constructed native promoter (*pATG8a*)-driven GFP reporters, *pATG8a*:CS-GFP and *pATG8a*:CL-GFP, with *GFP* preceded by 5′ UTRs of *ATG8a(S)* and *ATG8a(L)*, respectively (Fig. 5a). GFP reporter assays were performed by introducing the constructs into protoplasts from wild-type plants that were either unexposed (control) or exposed to HS for 2 h (Fig. 5b). Since protoplast isolation and transfection proceeded at 23 °C, this period was regarded as the post-HS recovery phase. As determined by immunoblotting with the anti-GFP antibody, the translational activity of *ATG8a(L)* 5′ UTR (CL) was ~17-fold higher (1:0.06 ratio) than that of *ATG8a(S)* 5′ UTR (CS) in post-HS protoplasts, while this difference was not shown in control protoplasts (Fig. 5c).

To further evaluate whether *ATG8a(S)*- and *ATG8a(L)*-specific S and L sequences in 5′ UTRs are critical for differential translation of ATG8a(S) and ATG8a(L) during HS recovery, we constructed *pATG8a*:CLS-GFP with both L and S sequences and *pATG8a*:C-GFP with only the common C sequence (Fig. 5a). Their expression was then compared with that of *pATG8a*:CS-GFP and *pATG8a*:CL-GFP (Fig. 5d). In post-HS protoplasts, CLS-GFP translation was stimulated to a level close to that of CL-GFP, while C-GFP was expressed at a much lower

https://doi.org/10.1038/s41467-025-61191-5

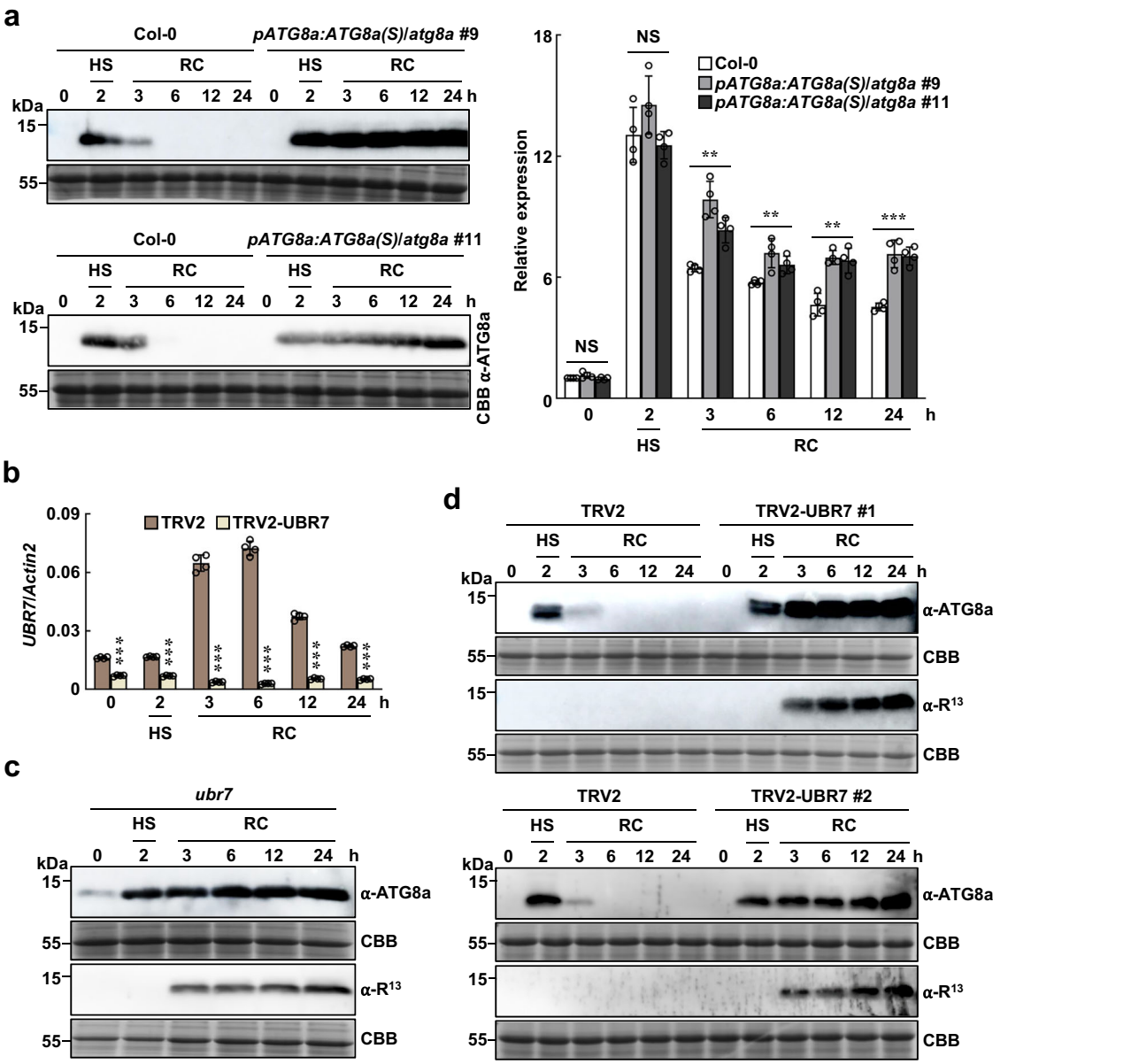

Fig. 6 | ATG8a degradation is UBR7-dependent during HS recovery. a Sustained ATG8(S) expression is tolerant to proteasomal degradation during HS recovery. Protein (left) and transcript (right) levels of ATG8a were determined in Col-0 and *pATG8:ATG8a(S)/atg8a* plants by immunoblotting and RT-qPCR, respectively. Data represent means ± SD ($n = 4$ biological replicates). Asterisks indicate significant differences between Col-0 and *pATG8:ATG8a(S)/atg8a* plants (Two-tailed Student's *t* test; $^{***}P < 0.001$; $^{**}P < 0.01$; The *P* value are as follows. 0.1144, 0.4537 in 0 h; 0.1865, 0.5309 in 2 h; 0.0003, 0.0011 in 3 h; 0.0074, 0.008 in 6 h; 0.0004, 0.0019 in 12 h; 0.0003, 0.0001 in 24 h, respectively. NS not significant. **b** *UBR7* is highly induced during HS recovery but suppressed by VIGS. *UBR7* transcript levels were analyzed by RT-qPCR in TRV2 control and TRV2-UBR7 plants exposed to HS (42 °C) for 2 h and recovery (23 °C) for the indicated times. Data represent means ± SD ($n = 4$ biological replicates). Asterisks indicate significant differences between TRV2 and TRV2-UBR7 plants (Two-tailed Student's *t* test; $^{***}P < 0.001$; $P < 0.0001$ in all indicated points). **c, d** ATG8a degradation is UBR7-dependent during HS recovery. ATG8a expression was monitored during HS and recovery in *ubr7* (**c**) and TRV2 and TRV2-UBR7 (**d**) plants. α-R^{13}, anti-R^{13}-ATG8a antibody. ATG8a proteins were analyzed by immunoblotting with respective antibodies (**a**, **c**, **d**), and Coomassie brilliant blue (CBB) staining served as a loading control (**a**, **c**, **d**). Three independent experiments were repeated with similar results (**a**, **c**, **d**). HS heat stress (**a**–**d**); RC recovery (**a**–**d**).

level, comparable to that of CS-GFP (Fig. 5d). *GFP* transcripts accumulated at similar levels across different constructs (Fig. 5c, d). These results suggest that the L sequence of *ATG8a*(*L*) 5′ UTR has a stimulatory effect on translation of *ATG8a*(*L*) and significantly increases ATG8a(L) abundance during HS recovery.

ATG8a degradation is UBR7-dependent during thermorecovery

To further validate whether ATG8a(L) is responsible for ATG8a degradation during the HS recovery period, we generated *ATG8a*(*S*)-expressing *pATG8:ATG8a*(*S*)/*atg8a* complementation lines, in which the native promoter-driven *ATG8a*(*S*) is introduced into *atg8a* mutant and subjected them to HS and recovery conditions (Fig. 6a). In these complementation lines, ATG8a expression remained high throughout both HS and recovery phases, implying that the decrease in ATG8a abundance after HS is due to ATG8a(L) production, followed by subsequent degradation. RT-qPCR analysis showed that the transcript levels of *ATG8a* in *pATG8:ATG8a*(*S*)/*atg8a* plants are higher than in wild-type plants during the HS recovery phase (Fig. 6a). Since transcripts from the *ATG8a*(*S*) transgene lack UTRs, which may influence mRNA stability and abundance, ATG8a(S) accumulation during HS

recovery could be partially attributed to increased expression in transgenic lines.

To determine whether ATG8a degradation is UBR7-dependent, further tests were conducted in *ubr7* mutant and *UBR7*-silenced lines (TRV2-UBR7) generated by tobacco rattle virus (TRV)-based virus-induced gene silencing (VIGS)[51,52]. VIGS was successful, leading to a 56–96% reduction of *UBR7* transcripts in TRV2-UBR7 lines compared to the TRV2 control, with significant induction of *UBR7* during thermo-recovery (Fig. 6b). Consistently, no reduction in ATG8a protein levels was observed in both *ubr7* and TRV2-UBR7 plants, and R^{13}-ATG8a proteins accumulated after release from HS (Fig. 6c, d). These results demonstrate that the decrease in ATG8a protein abundance after HS is due to ATG8a(L) expression, which occurs through the UBR7-mediated N-degron pathway.

Next, we assessed autophagy activation during HS and recovery. ATG8a expression in wild-type and *pATG8:ATG8a*(*S*)/*atg8a* plants correlated with the formation of active ATG8a, i.e., the ATG8a-PE conjugate (Fig. 7a). Consistent with previous observations[53], ATG8a-PE conjugation was markedly reduced in *atg5-1* and *atg7-2* mutants. Moreover, the formation of autophagosomes, a hallmark of autophagy activation, was monitored in transgenic plants expressing GFP-tagged SH3 DOMAIN-CONTAINING PROTEIN2 (SH3P2), a reliable autophagosome marker localized to the autophagosome membrane[54]. Double immunostaining with anti-GFP and either anti-ATG8a or anti-R^{13}-ATG8a antibodies showed a strong accumulation of SH3P2-GFP-positive puncta during both HS and recovery. However, ATG8a-positive autophagic structures were detected only under HS (Fig. 7b, c). Notably, MG132 treatment restored the accumulation of ATG8a- and R^{13}-ATG8a-positive puncta during HS recovery, aligning with their expression patterns (Fig. 4e).

These results suggest that while ATG8a functions in HS-induced autophagy, other ATG8 isoforms may replace ATG8a to participate in autophagy during HS recovery. Thus, we analyzed the expression of other *ATG8s* during HS responses, especially whether their expression increases after HS release. Supporting our idea, *ATG8b*, *ATG8d*, and *ATG8g* were significantly induced during HS recovery (Supplementary Fig. 8a).

ATG8a turnover is required for tolerance to recurring HS in *Arabidopsis*

To assess the role of ATG8a in HS responses, we additionally constructed transgenic lines of *atg8a* complemented with *ATG8a* genomic DNAs containing either the wild-type sequence (*gATG8a*/*atg8a*) or a G to A mutation at the 5′ splice site of the retained intron in ATG8a(L) (*gATG8a*^{PM}/*atg8a*), which exclusively produces *ATG8a*(*L*) (Supplementary Fig. 8b). We then examined how these genomic DNA complementation lines express ATG8a during HS and recovery. As expected, *gATG8a*/*atg8a* lines exhibited the same ATG8a expression patterns as wild-type plants at both RNA and protein levels (Supplementary Fig. 8c, d). However, *gATG8a*^{PM}/*atg8a* lines failed to express *ATG8a*(*S*) (Supplementary Fig. 8c) and barely produced ATG8a proteins under HS, but expressed degradable ATG8a(L) during HS recovery (Supplementary Fig. 8d). Under HS, the aberrantly generated *ATG8a(L)* transcripts, due to the failure of intron removal, appear to be destabilized in *gATG8a*^{PM}/*atg8a* lines.

In nature, temperature fluctuates during the day and night, exposing plants to repeated daily HS and recovery, particularly during hot summer days. To examine ATG8a expression under such conditions, plants were grown at 23 °C under long-day conditions (16-h light/8-h dark cycle) with 12-h HS at 42 °C in the middle of the day. Notably, the increase and decrease in ATG8a levels during HS and recovery were repeated daily (Fig. 8a). Recurring ATG8a turnover was also evident under short-day conditions (8-h light/16-h dark cycle) with 8-h HS during the day (Supplementary Fig. 9a). ATG8a expression was not detectable during the day and night under normal conditions, indicating that daily changes in ATG8a abundance do not correlate with circadian rhythm.

Next, *atg8a*, *ubr7*, TRV2-UBR7, and all complementation lines were subjected to repeated daily HS and recovery for 5 days and evaluated for thermotolerance. Based on the ATG8a levels, they can be divided into three classes: (1) *atg8a* null mutant, (2) *gATG8a*^{PM}/*atg8a* lines with defective ATG8a under HS (Supplementary Fig. 8d), and (3) *ubr7*, TRV2-UBR7, and *pATG8:ATG8a*(*S*)/*atg8a* lines with high ATG8a expression (Fig. 6a, c, d). Unlike wild-type and *gATG8a*/*atg8a* plants, which remained green, all other tested plants exhibited reduced thermotolerance under both long-day and short-day conditions; their leaves turned yellow with a significant decrease in chlorophyll content (Fig. 8b–e, Supplementary Fig. 9b–e). These results suggest that daily ATG8a turnover is important for plant response to recurring HS and recovery, and that abnormally low or excessive ATG8a expression both impair plant thermotolerance.

Proteomic analysis reveals ATG8a-dependent altered abundance of HS-responsive proteins during HS recovery

Previous studies report that autophagy is critical for degradation of thermo-sensitive proteins and HSPs during both the HS and recovery periods[49,50,55,56]. In this study, we showed that HS-upregulated ATG8a abundance decreases and other *ATG8s* such as *ATG8b*, *ATG8d*, and *ATG8g* are activated after release from HS (Fig. 4c, d, Supplementary Fig. 8a). This implies that other ATG8 isoforms may replace ATG8a to induce autophagic protein degradation during HS recovery. The results of previous and our studies led us to hypothesize that autophagic cargo to be cleared may change at different stages of HS responses and be recognized by ATG8a and other ATG8s that are differentially expressed during the HS and recovery periods.

Based on our speculation that ATG8 isoforms differentially target autophagic cargo during distinct stages of HS responses, we aimed to identify proteins whose clearance is disturbed by sustained ATG8a expression during HS recovery. For this, we analyzed proteomes of wild-type and *pATG8:ATG8a*(*S*)/*atg8a* (#9) plants subjected to HS and recovery using label-free liquid chromatography-tandem mass spectrometry (LC-MS/MS) (Supplementary Data 1). Significant changes in protein expression were defined according to the cutoff criteria (adjusted $P < 0.05$, $\log_2$ fold change ($|\log_2 FC| \geq 1$). HS-responsive proteins were first identified by analyzing differentially expressed proteins (DEPs) between control (no treatment, NT) and HS treatment, revealing 149 (93 increased and 56 decreased) and 133 (85 increased and 48 decreased) DEPs (HS-DEPs) in wild-type and *pATG8:ATG8a*(*S*)/*atg8a* plants, respectively (Fig. 9a, b, Supplementary Data 2). All HS-DEPs in *pATG8:ATG8a*(*S*)/*atg8a* plants overlapped entirely with those in wild-type plants, meaning that the HS response of *pATG8:ATG8a*(*S*)/*atg8a* plants is essentially the same as that of wild-type plants. The upregulated HS-DEPs were then subjected to Gene Ontology (GO) enrichment analysis using GO Biological Process (BP) terms provided by the PANTHER database (http://pantherdb.org) (Supplementary Data 3). The top significant GO terms indicated that the upregulated HS-DEPs in wild-type and *pATG8:ATG8a*(*S*)/*atg8a* plants are commonly involved in biological processes such as heat response and protein folding (Fig. 9c). These results further suggest that ATG8a(S) acts as a major ATG8 in HS-activated autophagy.

Next, we analyzed proteins (RC-DEPs) that are differentially expressed between wild-type and *pATG8:ATG8a*(*S*)/*atg8a* plants during HS recovery (Supplementary Data 4). Of the identified RC-DEPs, the majority (183 of 202, 91%) were up-regulated in *pATG8:ATG8a*(*S*)/*atg8a* plants, as displayed in the volcano plot (Fig. 9d). The GO analysis of RC-DEPs revealed that 183 up-regulated RC-DEPs are enriched in BP terms of heat response and protein folding (Fig. 9e, Supplementary Data 5), similar to the upregulated HS-DEPs. A heatmap was generated to show the changes in protein abundance among NT, HS, and recovery conditions (Supplementary Fig. 10). The proteomic profiles revealed that

https://doi.org/10.1038/s41467-025-61191-5

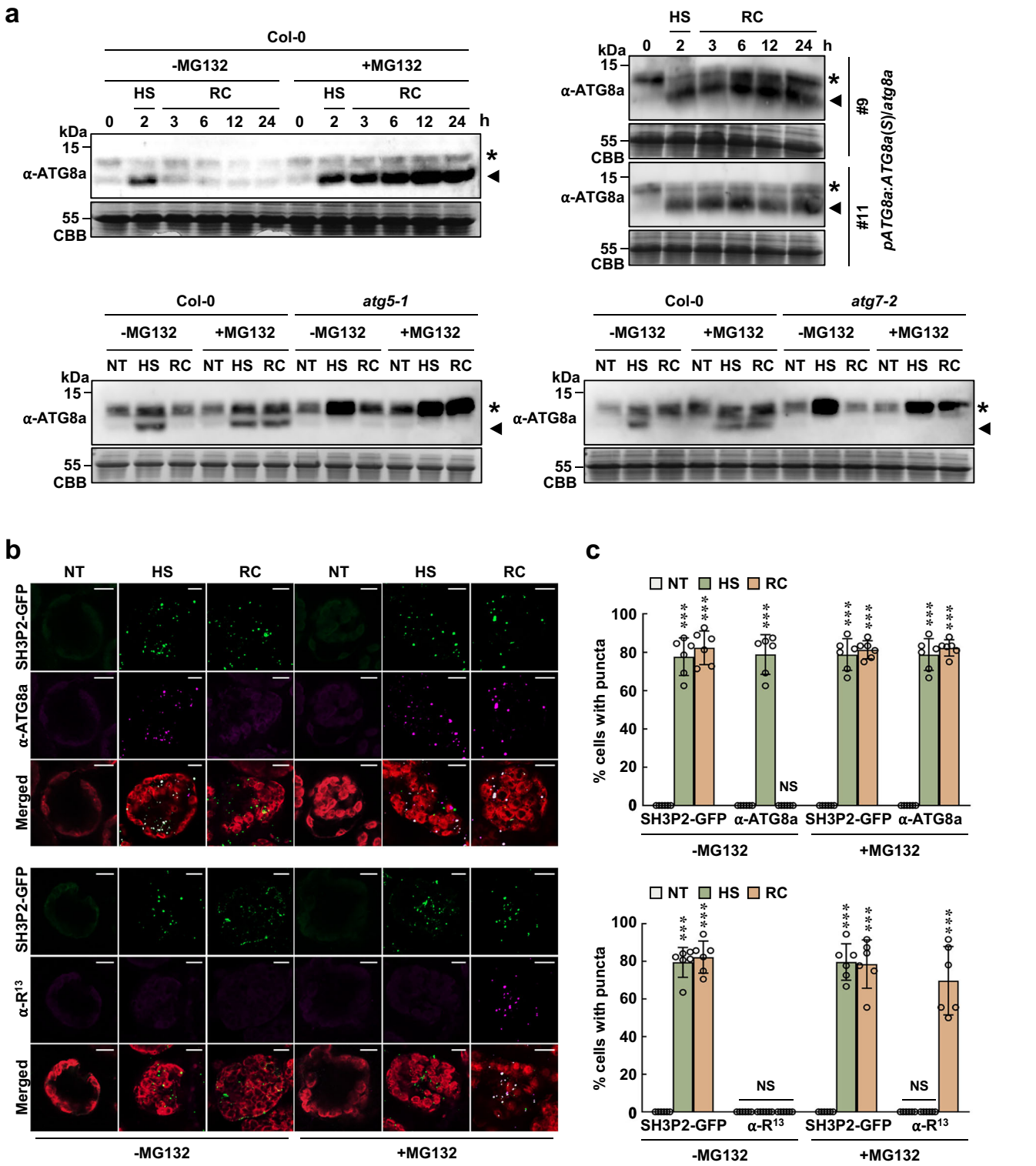

Fig. 7 | Autophagic activation during HS and recovery. a ATG8a lipidation assay. Protein extracts were prepared from Col-0, *atg5-1*, *atg7-2*, and *pATG8:ATG8a(S)/atg8a* plants exposed to HS (42 °C) for 2 h and recovery (23 °C) for the indicated times. For MG132 treatment, plants were sprayed with MG132 (10 μM) and incubated for 1 h prior to exposure to HS and recovery conditions. Proteins were separated by SDS-PAGE in the presence of 6 M urea. ATG8a proteins were analyzed by immunoblotting with the anti-ATG8a antibody, and Coomassie brilliant blue (CBB) staining served as a loading control. Asterisks and arrowheads indicate ATG8a and ATG8a-PE, respectively. Three independent experiments were repeated with similar results. **b** Double immunostaining with the anti-GFP/anti-ATG8a (upper) and anti-GFP/anti-R^{13}-ATG8a (lower) antibodies for autophagic structures in SH3P2-GFP plants exposed to HS (42 °C) for 2 h and recovery (23 °C) for 6 h. For MG132 treatment, plants were sprayed with MG132 (10 μM) and incubated for 1 h prior to exposure to HS and recovery conditions. Five independent experiments were repeated with similar results. Bars, 10 μm. **c** Quantification of cells with GFP/ATG8a/R^{13}-ATG8a-positive autophagic puncta in (**b**). Stained leaves were photographed and cells with fluorescent spots were counted per 250 μm^2 area. Results represent means ± SD ($n = 6$ microscopic images). Asterisks indicate significant differences from the respective NT (Two-tailed Student's *t* test; $^{***}P < 0.001$; $P < 0.0001$ in all indicated points). NS not significant. NT no treatment (**b**, **c**); HS heat stress (**a**–**c**); RC recovery (**a**–**c**).

https://doi.org/10.1038/s41467-025-61191-5

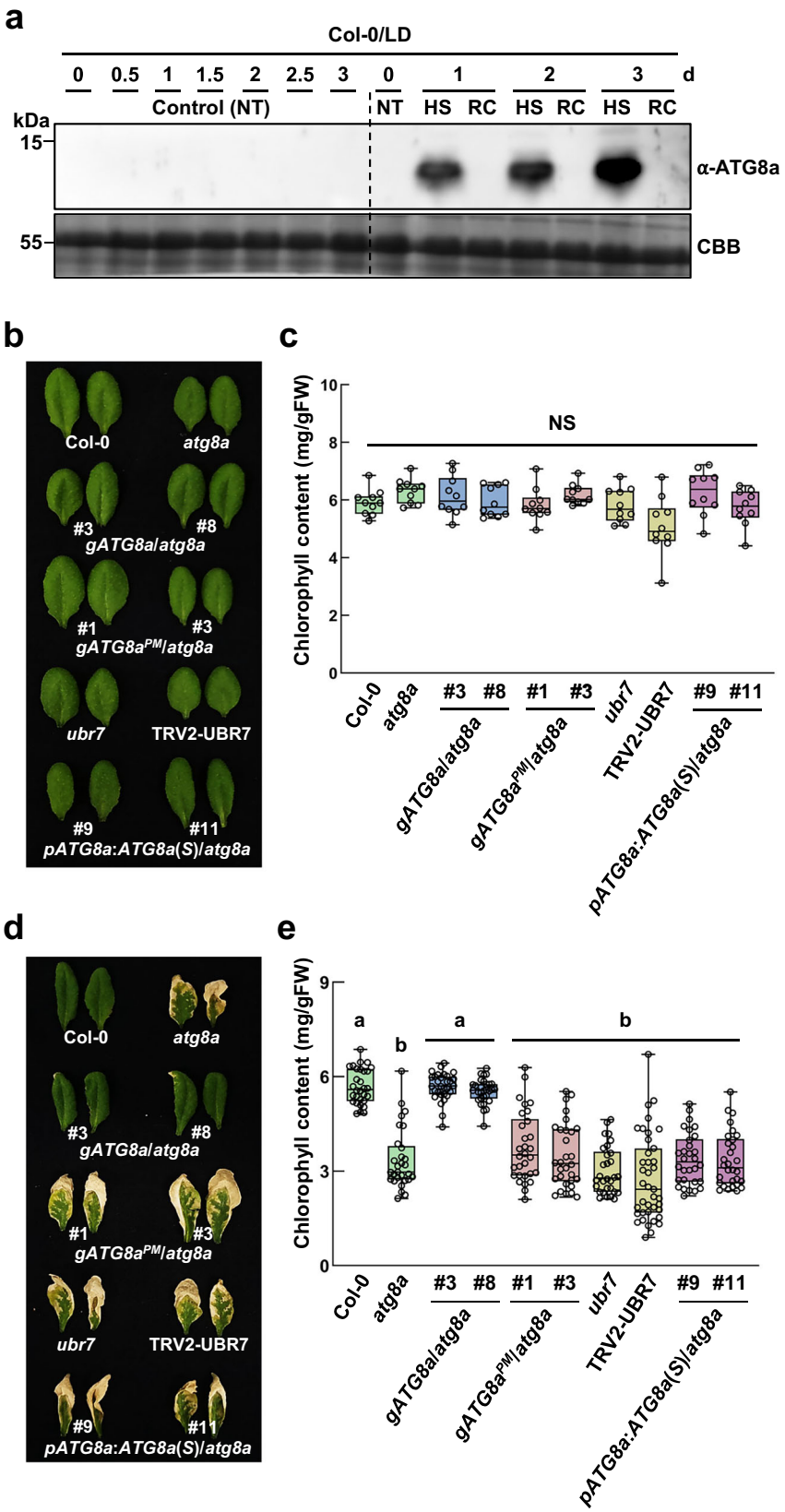

15 upregulated HS-DEPs are decreased in wild-type but remain upregulated in *pATG8:ATG8a(S)/atg8a* plants during HS recovery (Fig. 9f, Supplementary Data 6). Among them, two HSPs, HSP70-4 and HSP17.6II, and fibrillin FBN1a[57,58] were annotated to the GO term for response to heat. Together, these results support our hypothesis that sustained ATG8a expression may interfere with the clearance of HS-induced proteins, including HSPs, which would otherwise disappear in wild-type plants during HS recovery.

Discussion

In this study, we demonstrate that ATG8a stability is regulated by the Arg/N-degron pathway, resulting in the removal of ATG8a proteins.

Fig. 8 | ATG8a turnover is important for plant thermotolerance. a Fluctuations in ATG8a abundance coincide with daily HS and recovery cycles. Col-0 plants grown in long days were exposed to 42 °C (HS) for 12 h during the day and maintained at 23 °C (recovery) for the remaining 12 h. Total proteins were extracted from Col-0 plants exposed to HS and recovery repeatedly for 3 days and analyzed by immunoblotting with the anti-ATG8a antibody. Coomassie brilliant blue (CBB) staining served as a loading control. Three independent experiments were repeated with similar results. LD long day, NT no treatment, HS heat stress, RC recovery. **b** Leaf phenotypes of Col-0, *atg8a*, *ubr7*, TRV2-UBR7, and complementation lines grown in long days. Plants were maintained at 23 °C under long-day conditions during HS experiments. **c** Quantification of chlorophyll content in control plants in (**b**). Data represent means ± SD ($n = 10$ leaves). Boxplots indicate median (box center line), 25%, 75% (box), and 5%, 95% (whiskers). NS not significant. **d** Thermotolerance phenotypes of Col-0, *atg8a*, *ubr7*, TRV2-UBR7, and complementation lines under recurring HS and recovery conditions. Plants grown in long days were exposed to 42 °C (HS) for 12 h during the day and maintained at 23 °C (recovery) for the remaining 12 h, which was repeated for 5 days. Plants were allowed to recover for an additional 3 days and observed for leaf phenotypes. **e** Quantification of chlorophyll content in plants exposed to HS and recovery in (**d**). Data represent means ± SD ($n = 32$ leaves). Different letters indicate significant differences (One-way ANOVA with Tukey's HSD test; $P < 0.05$). Boxplots indicate median (box center line), 25%, 75% (box), and 5%, 95% (whiskers).

ATG8a pre-mRNAs are alternatively spliced to produce two splice variants *ATG8a*(*S*) and *ATG8a*(*L*), with *ATG8a*(*L*) being an IR variant encoding N-degron-bearing ATG8a. *ATG8a*(*S*) and *ATG8a*(*L*) exhibit differential expression patterns, coinciding with timely fluctuations in ATG8a abundance. We propose a molecular mechanism for plant adaptation to HS via N-degron-mediated proteolytic regulation ATG8a (Fig. 10).

Our results indicate that AS is crucial for dynamic changes in ATG8a abundance during HS responses (Fig. 4a–c). AS is a post-transcriptional regulatory process that enhances the functional diversity of proteins and plays an important role in plant responses to abiotic stress[59]. Among AS events, IR is the most frequent one in plants, while exon skipping is prevalent in mammals[60]. Many studies have addressed the role of AS in plant HS responses through the generation of active splice isoforms of heat-responsive regulators, including heat shock transcription factors (HSFs)[61,62]. Our finding makes an important contribution to these studies, demonstrating that AS provides a means of fine-tuning gene expression in response to HS. We also found that AS generates different 5′ UTRs in *ATG8a*(*S*) and *ATG8a*(*L*) variants, with a specific sequence (designated as L) in *ATG8a*(*L*) 5′ UTR enhancing translational efficiency. This is a plausible mechanism for the increased production of ATG8a(L) proteins during the post-HS period (Fig. 5). Further investigations are required to identify *cis*-RNA elements and *trans*-factors that promote translation of *ATG8a*(*L*) transcripts.

UBR7 was previously identified as a histone H2B monoUb ligase in plants and mammals[43,63,64]. In addition, TurboID-based proximity labeling identified UBR7 as a regulator of the tobacco N immune receptor[65]. Our results provide the first line of evidence that UBR7 acts as an N-recognin and, like other UBRs, recognizes ATG8a(L) with an N-terminal Arg through the UBR box domain. It would be worth investigating whether UBR7 can also recognize other type I and even type II N-degrons. Notably, while ATG8a(L) proteins localize in both the cytosol and nucleus, UBR7 is expressed and interacts with ATG8a(L) in the nucleus (Fig. 3d, Supplementary Fig. 3f, 4), suggesting that N-degron-mediated ATG8a degradation occurs in the nucleus. Given that ATG8s are synthesized as cytosolic factors and are involved in autophagosome biogenesis, the spatial separation of ATG8a activation (in the cytosol) and degradation (in the nucleus) may be necessary to prevent interference between these two opposing processes. We also show that N-terminal cleavage of ATG8a(L) is a prerequisite for UBR7-mediated polyubiquitination and degradation (Fig. 2, Supplementary Fig. 5). A number of N-degron substrates are created through decapping[3,19,20,22,66,67] or endoproteolytic cleavage[8,19,68–74]. Given that the *Arabidopsis* genome contains over 700 genes encoding putative proteases[75], the specific protease(s) for endoproteolytic processing of ATG8a(L) remains to be determined.

Autophagy provides the most effective way to remove protein aggregates and damaged organelles and plays a homeostatic role in plants exposed to abiotic stress, including HS[50]. We propose that ATG8a degradation may be necessary to replace ATG8a with other ATG8s (e.g., ATG8b, ATG8d, and ATG8g) (Supplementary Fig. 8a), enabling distinct ATG8s and their interacting cargo receptors to selectively target different cargo in the process of selective autophagy during HS and recovery (Fig. 10). Previous studies have shown that autophagy receptors determine the specificity of cargo, and their interactions with ATG8 isoforms vary depending on cargo and biological processes involved[76]. The proposed mechanism is supported by our proteomics results, which show that HS-upregulated proteins decrease in wild-type plants but remain high in *pATG8:ATG8a*(*S*)/*atg8a* plants during the HS recovery phase (Fig. 9d, f). We speculate that sustained ATG8a expression interferes with the actions of other ATG8(s) in *pATG8:ATG8a*(*S*)/*atg8a* plants, thereby preventing degradation of heat-responsive proteins, including HSPs, which would otherwise decrease in abundance in wild-type plants released from HS. Our findings are consistent with previous studies, in which autophagy is directed at distinct targets during HS and recovery, mediating selective degradation of HSPs during the recovery phase[49,56]. The removal of heat-responsive proteins during HS recovery may be required to reset stress conditions and enhance resistance to upcoming HS. A recent study reveals a non-canonical role of ATG8s in Golgi reassembly after HS[77]. Whether proteolytic regulation of ATG8a is related to organellar recovery in plant response to HS remains to be explored.

In nature, plants are exposed to day and night temperature fluctuations, subjecting them to daily HS and recovery conditions. The increase and decrease in ATG8a abundance coincided with HS and recovery cycles, and abnormally low (*atg8a* and *gATG8a*^{PM}/*atg8a* lines) and high (*ubr7*, TRV2-UBR7, and *pATG8:ATG8a*(*S*)/*atg8a* lines) levels of ATG8 expression both impaired plant thermotolerance (Fig. 8, Supplementary Fig. 9), implying that ATG8a fluctuations are critical for plant thermotolerance. Intriguingly, early studies on crops have reported that plants undergo a diurnal cycle of heat resistance, which peaks during the day and decreases at night[78]. This is consistent with findings that a diurnal pattern of thermotolerance correlates with diurnal expression of *HSP* genes[79]. Together, our findings demonstrate that the N-degron pathway is a critical mechanism for timely and quantitative regulation of ATG8a and, ultimately, heat-responsive proteins over daily thermocycles. This dynamic regulation may have evolved as a survival strategy for plants to cope with environmental thermal changes.

Methods

Plant materials and growth conditions

Arabidopsis thaliana (Ecotype Columbia, Col-0) plants were grown at 23 °C under long-day conditions in a 16-h light/8-h dark cycle and short-day conditions in an 8-h light/16-h dark cycle. The mutant lines used in this study are *prt6-1* (SALK_004079), *big-3* (SALK_107817)[80], *ubr7* (SALK_034619), *atg8a* (SALK_045344), *atg5-1* (SAIL_129_B07), and *atg7-2* (GABI_655B06) from the Arabidopsis Biological Resource Center (ABRC). T-DNA insertion sites were verified by sequence analysis using gene-specific primers (Supplementary Data 7). To generate *pATG8:ATG8a*(*S*)/*atg8a* plants, the *ATG8a*(*S*) coding region was cloned into the pCAMBIA3300 binary vector under the control of the native p*ATG8a* promoter (−1 to −1150 bp relative to the transcription start site) amplified from *Arabidopsis* genomic DNA by PCR.

https://doi.org/10.1038/s41467-025-61191-5

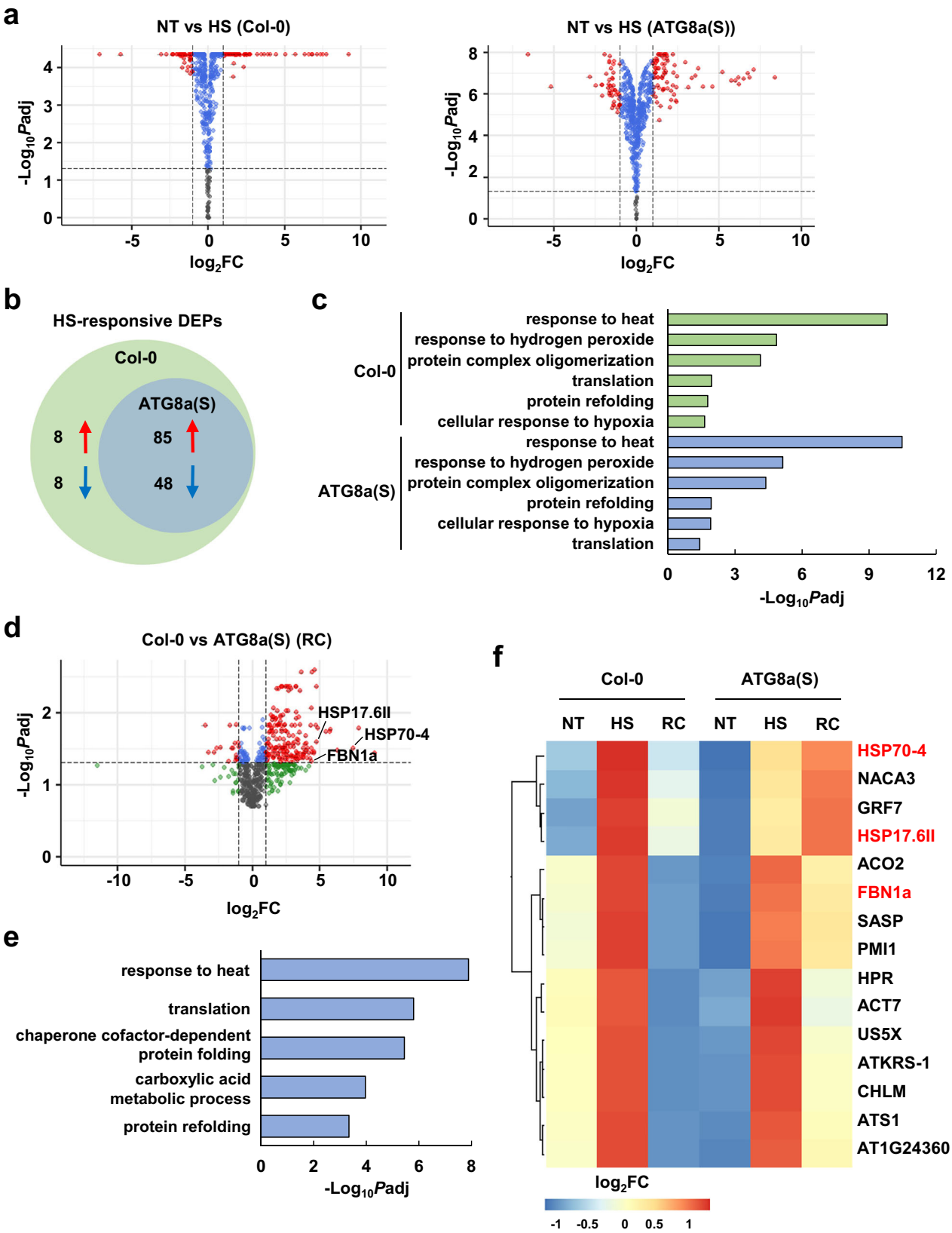

To generate *gATG8a*/*atg8a* and *gATG8a*^{PM}/*atg8a* plants, the 2572-bp genomic DNA region containing *ATG8a* was amplified by PCR, and a G to A mutation was made by site-directed mutagenesis using primers in Supplementary Data 7. The constructs were transformed into *atg8a* plants via *Agrobacterium tumefaciens* GV3101 using the floral dip method[1].

Plant treatments

For chemical treatments, *Arabidopsis* protoplasts were treated with MG132 (10 μM with 0.1% DMSO) and cycloheximide (100 μM with 0.1% DMSO) for 3 h and ConA (1 μM with 0.1% DMSO) for 16 h before sampling. Four-week-old plants were sprayed with MG132 (10 μM with 0.1% DMSO) or syringe-infiltrated with DTT (8 mM in

Fig. 9 | Proteomics reveals that ATG8a expression alters protein profiles during HS recovery. a Volcano plots of DEPs between no treatment (NT) and HS in Col-0 and *pATG8:ATG8a*(*S*)/*atg8a* plants. Cutoff values (*P*adj = 0.05 and $|\log_2 FC| = 1$) are indicated by dashed lines based on *P* value of significance <0.05. *P* values were calculated using two-tailed Student's *t* test. Red dots represent significantly upregulated and downregulated DEPs. Volcano plots were generated using the EnhancedVolcano package in R Studio. **b** Venn diagrams for HS-responsive DEPs in Col-0 and *pATG8:ATG8a*(*S*)/*atg8a* plants. **c** GO enrichment analysis of HS-upregulated DEPs in Col-0 and *pATG8:ATG8a*(*S*)/*atg8a* plants. The 6 most significantly (FDR < 0.05) enriched GO terms in the Biological Process are presented based on *P* value of significance <0.05 for HS-upregulated DEPs. *P* values were calculated using two-tailed Student's *t* test. **d** Volcano plots of DEPs between Col-0 and *pATG8:ATG8a*(*S*)/*atg8a* plants during HS recovery (RC). Cutoff values (*P*adj = 0.05 and $|\log_2 FC| = 1$) are indicated by dashed lines based on *P* value of significance <0.05. *P* values were calculated using two-tailed Student's *t* test. Red dots represent significantly upregulated and downregulated DEPs. Volcano plots were generated using the EnhancedVolcano package in R Studio. **e** GO enrichment analysis of DEPs between Col-0 and *pATG8:ATG8a*(*S*)/*atg8a* plants during RC. The 5 most significantly (FDR < 0.05) enriched GO terms in the Biological Process are presented based on *P* value of significance <0.05. *P* values were calculated using two-tailed Student's *t* test. **f** Heatmap showing expression profiles of 15 selected DEPs between Col-0 and *pATG8:ATG8a*(*S*)/*atg8a* plants under NT, HS, and RC. Selected proteins were HS-upregulated DEPs that decreased in Col-0 but remained high in *pATG8:ATG8a*(*S*)/*atg8a* plants during RC. Protein information is provided in Supplementary Data 6. Heatmap was generated using the pheatmap package in R Studio. FC fold change (**a, d**); NT no treatment (**a**, **f**); HS heat stress (**a**, **b**, **f**); RC recovery (**d**, **f**); ATG8a(S), *pATG8:ATG8a*(*S*)/*atg8a* plants (**a**–**d**, **f**).

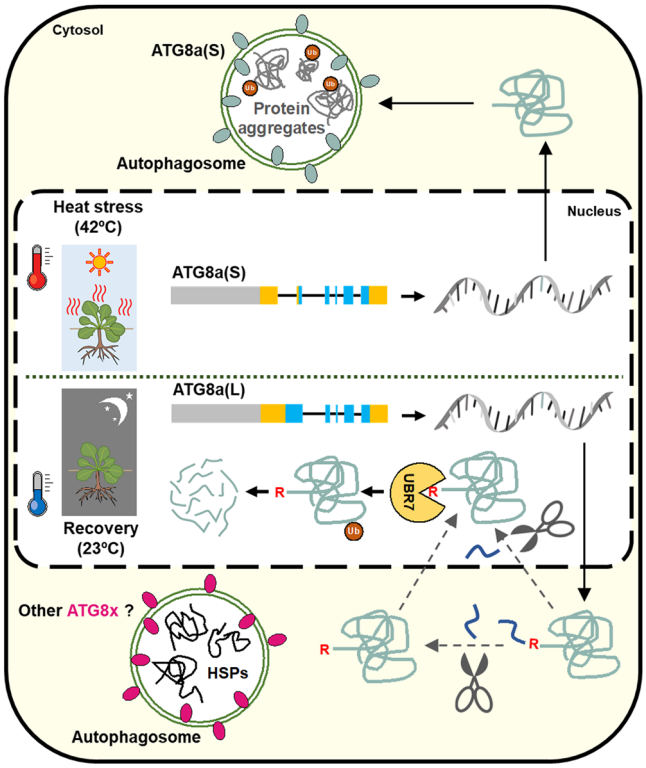

Fig. 10 | A model for N-degron-mediated regulation of ATG8a and diurnal thermotolerance. *ATG8a* pre-mRNAs are alternatively spliced to generate two splice variants *ATG8*(*S*) and *ATG8a*(*L*), which accumulate mainly during HS and recovery, respectively. ATG8a(L) is N-terminally processed to expose the Arg/N-degron, which is recognized by the N-recognin UBR7, leading to polyubiquitination and subsequent proteasomal degradation of ATG8a. Eventually, ATG8a and other ATG8 isoforms (ATG8x) may participate in selective autophagy, targeting different cargos, e.g., protein aggregates and HSPs, during HS and recovery phases, respectively. These fluctuations in ATG8a abundance coincide with daily thermocycles, enhancing thermotolerance in plants.

H_2O), TM (250 ng/ml with 0.1% DMSO), and ConA (1 μM with 0.1% DMSO), and incubated for the indicated times. HS experiments were performed as previously described[81]. For expression analysis, 4-week-old plants were exposed to 42 °C (HS phase) and then incubated at 23 °C (recovery phase) for the indicated times in an incubator. For phenotype and chlorophyll content analysis, HS treatment at 42 °C was performed for 8 or 12 h during the day on 4-week-old plants grown under short-day or long-day conditions, respectively, which was repeated for 5 days. Plants were allowed to recover for an additional 3 days before further analysis.

Gene expression analysis

Total RNAs were extracted from *Arabidopsis* leaves using TRIzol reagent (Meridian Bioscience), treated with DNase I (New England Biolabs), and reverse-transcribed into cDNAs using PrimeScript RT reagent kit (TaKaRa). Quantitative real-time PCR (RT-qPCR) was performed using KAPA SYBER FAST qPCR master mix (Kapa Biosystems) with gene-specific primers (Supplementary Data 7) on a LightCycler 480 system (Roche) according to the manufacturer's protocol. *Actin2* was used as the reference gene for normalization. Data were analyzed using LC480 Conversion and LinRegPCR software (Heart Failure Research Center).

Transient expression assay

Various expression constructs were generated for transient expression assays in *Arabidopsis* protoplasts. For protein expression constructs, coding regions of *ATG8a*, *ATG8e*, *UBR7*, and *Ub* were amplified from the *Arabidopsis* cDNA library by PCR and cloned into pUC19 vectors containing CaMV 35S promoter, *RBCS* terminator, and the indicated tag sequences. Deletion and substitution mutations were introduced into *ATG8a* by site-directed mutagenesis using primers in Supplementary Data 7. For 5′ UTR-driven reporter (translational efficiency) constructs, the *GFP* sequence was fused with the indicated 5′ UTR sequences of *ATG8a*(*S*) and *ATG8a*(*L*) and the 3′ UTR sequence of *ATG8a*, and cloned into the pUC19 vector containing p*ATG8a* promoter and *RBCS* terminator sequences. Ub fusion constructs, Ub-R^{13}-ATG8a, Ub-A^{13}-ATG8a, Ub-R-GUS-FLAG, and Ub-M-GUS-FLAG, were generated through a DNA synthesis service at Bionics and cloned into pUC19 vectors containing CaMV 35S promoter and *RBCS* terminator.

Arabidopsis mesophyll protoplasts were isolated and transfected as previously described in ref. 52. Leaves were sliced and incubated for 3 h in an enzyme solution (20 mM MES-KOH, pH 5.7, 1% cellulase R-10, 0.4% macerozyme R-10, 0.4 M D-mannitol, 20 mM KCl, 10 mM $CaCl_2$, and 0.1% BSA). Protoplasts were collected by filtering through a 70-μm cell strainer, centrifuged, and resuspended in W5 solution (1.5 mM MES-KOH, pH 5.6, 154 mM NaCl, 125 mM $CaCl_2$, and 5 mM KCl). Isolated protoplasts (2×10^4) were transfected with 15 μg of *ATG8a* and *ATG8e*, 20 μg of *UBR7*, 10 μg of *Ub*, 15 μg of 5′ UTR reporters, 20 μg of BiFC constructs, and 10 μg of Ub fusion constructs. After transfection, protoplasts were incubated at room temperature overnight to allow expression.

Antibody preparation

A rabbit polyclonal antibody specific for R^{13}-ATG8a was generated using the peptide RIAMAKSSFKI corresponding to the N-terminal sequence (positions 13–23) of ATG8a through a custom service at AbFrontier as previously described in ref. 26. Briefly, antisera from rabbits immunized with the peptide were subjected to affinity purification using the peptide RIAMAKSSFKI. The specificity of the purified antibody was validated by immunoblot analysis using R^{13}-ATG8a and A^{13}-ATG8a and the peptide competition assay.

Immunoblotting and co-immunoprecipitation

For immunoblotting, total proteins were extracted by boiling protoplasts and ground plant leaves with liquid nitrogen in 6x sample buffer (100 mM Tris-HCl, pH 6.8, 12% SDS, 20% glycerol, 6% β-mercaptoethanol, and 0.2% bromophenol blue) for 10 min. For co-immunoprecipitation, protoplasts were lysed in lysis buffer (50 mM Tris-HCl, pH 7.4, 150 mM NaCl, 1% NP-40, and 1× protease inhibitor cocktail) for 30 min on ice. Lysates were centrifuged at 14,000 × *g* for 10 min at 4 °C, and the supernatant was incubated with the anti-HA antibody (Thermo Fisher Scientific) for 1 h at 4 °C. After an additional overnight incubation with Protein A agarose beads (Pierce), beads were washed with lysis buffer, and bound proteins were eluted by boiling in 6× sample buffer. Proteins were separated by SDS-PAGE and transferred to polyvinylidene fluoride membranes. For the separation of low molecular weight proteins, Tris-Tricine SDS-PAGE gels were utilized. Membranes were incubated with anti-HA (Thermo Fisher Scientific, 71-5500), anti-MYC (Abcam, ab32), anti-ATG8a (Abcam, ab77003), anti-Ub (Santa Cruz, sc-8017), anti-FLAG (Abcam, ab205606), anti-mCherry (Abcam, ab183628), and anti-GFP (Santa Cruz, sc-9996) antibodies. Antibody-bound proteins were detected by incubation with secondary antibodies conjugated to horseradish peroxidase using an enhanced chemiluminescence system (Amersham Biosciences).

Protein expression and purification

The coding regions of *ATG8a-i* were cloned into the modified pMAL2 vector containing the 6xHis and *FLAG* sequences to generate ATG8 fused to the N-terminal His and FLAG tags. The coding region of *UBR7* was cloned into the modified pMAL2 vector containing the *MYC* sequence to generate UBR7 fused to the N-terminal MYC tag. Substitution mutations for UBR7^{CM} were introduced into *UBR7* by site-directed mutagenesis using primers in Supplementary Data 7. *UBC8* encoding the *Arabidopsis* E2 enzyme was cloned into the pMAL2 vector to generate UBC8 fused to the N-terminal maltose-binding protein (MBP) tag. *Escherichia coli* BL21(DE3) pLysS cells were transformed with the constructs and cultured at 37 °C. Protein expression was induced by the addition of 0.3 mM isopropyl-β-D-thiogalactoside (IPTG) for 3 h at 28 °C. The cells were harvested and lysed by sonication in lysis buffer (50 mM Tris-HCl, pH 7.4, 400 mM NaCl, 5% glycerol, 1 mM $MgCl_2$, 5 mM Imidazole, 2 mM DTT, 0.5 mM PMSF, 1 mM NaF, 1 mM Na_3VO_4, and 1× protease inhibitor cocktail). His-FLAG-ATG8 proteins were purified using Ni-NTA agarose (QIAGEN), and MYC-UBR7 and MBP-UBC8 proteins were purified using anti-MYC (Pierce) and anti-MBP (New England Biolabs) magnetic beads, respectively, according to the manufacturer's instructions.

R^{13}-ATG8a and A^{13}-ATG8a proteins were prepared as previously described[16]. ATG8a was cloned into the modified pET vector to generate GST-LC3B-R^{13}/A^{13}-ATG8a fusion proteins. *E. coli* BL21(DE3) cells were transformed with the constructs and cultured at 37 °C. Protein expression was induced by the addition of 0.5 mM IPTG for 20 h at 18 °C. The cells were harvested and lysed by sonication in PBS buffer (137 mM NaCl, 2.7 mM KCl, 10 mM Na_2HPO_4, and 1.8 mM KH_2PO_4). The expressed proteins were purified using a Glutathione Sepharose HP column (Cytiva). The eluted proteins were loaded onto a HiTrap Q HP column (Cytiva) and eluted with a NaCl gradient up to 1 M. The GST-LC3B tag was cleaved with human ATB4B protease[82] overnight at 20°C and eliminated using a Glutathione Sepharose HP column (Cytiva). R^{13}/A^{13}-ATG8a proteins were further purified by size-exclusion chromatography using a HiLoad 16/600 Superdex 75 pg column (Cytiva).

In vitro pull-down assay

MYC-UBR7 (1 μg) was incubated with R^{13}/A^{13}-ATG8a (200 ng) in binding buffer (50 mM Tris-HCl, pH 7.4, 5 mM $MgCl_2$, and 30% glycerol) for 2 h at 4 °C. Anti-MYC antibody (Abcam, ab32) and protein G agarose beads (Pierce) were added and incubated for 2 h at 4°C. Bound proteins were eluted by boiling in 6x sample buffer, separated by SDS-PAGE, and visualized by immunoblotting with anti-ATG8a (Abcam, ab77003) and anti-MYC (Abcam, ab32) antibodies.

In vitro ubiquitination assay

In vitro ubiquitination assay was performed as previously described[83]. Recombinant MYC-UBR or MYC-UBR7^{CM} (500 ng) was incubated with either R^{13}-ATG8a or A^{13}-ATG8a (1 μg) in the presence of Ub (15 μg), human E1 UBE1 (50 ng; Merck), *Arabidopsis* E2 MBP-UBC8 (200 ng) in ubiquitination buffer (50 mM Tris-HCl, pH 7.4, 5 mM $MgCl_2$, 2 mM DTT, 4 mM ATP, and 1x protease inhibitor cocktail) for 3 h at 30 °C. Reactions were stopped by boiling in 6× sample buffer, and proteins were separated on a gradient gel (Invitrogen) by SDS-PAGE and detected by immunoblotting with anti-ATG8a (Abcam, ab77003), anti-MYC (Abcam, ab32), and anti-Ub (Santa Cruz, sc-8017) antibodies.

ATG8a lipidation assay

ATG8a lipidation assay was performed as previously described in ref. 53. Total proteins were extracted from 4-week-old plants exposed to HS and recovery conditions. Proteins were separated on 15% gels containing 6 M urea by SDS-PAGE, transferred to polyvinylidene fluoride membranes (Amersham Biosciences), and detected by immunoblotting with the anti-ATG8a antibody (Abcam, ab77003).

BiFC and subcellular localization

For BiFC, the full-length coding regions of *ATG8a*, *ATG8a* with the indicated mutations (*ATG8a^{R13A}* and *ATG8a^{3A}*), and *UBR7*, and the UBR domain region of *UBR7* were PCR-amplified using primers in Supplementary Data 7. The PCR products were cloned into pUC-SPYNE and pUC-SPYCE vectors[84] for the expression of fusion proteins UBR7-GFP^N, UBR-GFP^N, ATG8a-GFP^C, ATG8a^{R13A}-GFP^C, and ATG8a^{3A}-GFP^C. For subcellular localization, the PCR products of *UBR7* and *ATG8a* were cloned into pUC19 vectors containing the *GFP* and *mCherry* sequences for the expression of fusion proteins UBR7-GFP and ATG8a-mCherry. *Arabidopsis* protoplasts were transfected with these constructs and incubated for 20–24 h for protein expression. To visualize nuclei, protoplasts were treated with 3 μM DAPI (Merck) overnight. Fluorescent signals were observed using a confocal microscope (Zeiss LSM 700). Excitation and emission were set at 488/543 nm for GFP, 555/630 nm for mCherry, 639/710 nm for chlorophyll, and 350/465 nm for DAPI.

Immunostaining

Immunostaining was performed as described previously[85]. Leaf discs were fixed in 4% paraformaldehyde and 0.1% triton X-100 dissolved in PMEG buffer (50 mM PIPES, pH 6.9, 5 mM EGTA, and 5 mM $MgSO_4$) for 40 min at room temperature. Samples were washed with water and incubated in MES buffer (2 mM MES, pH 5.0, 0.2% driselase (Sigma), and 0.15% macerozyme R-10) for 20 min at 37 °C. Samples were then washed with PMEG buffer and incubated with anti-ATG8a (Abcam, ab77003), anti-GFP (Santa Cruz, sc-9996), and R^{13}-ATG8a antibodies in PMEG buffer containing 3% BSA overnight at 4 °C. After washing with PMEG buffer, samples were incubated with fluorescein isothiocyanate-conjugated goat anti-mouse IgG (AlexaFlour 488, Invitrogen) and fluorescein isothiocyanate-conjugated goat anti-rabbit IgG (AlexaFlour 488, 594, Invitrogen) for 3 h at room temperature. Images were acquired using a confocal microscope (Zeiss LSM 700) at 488/543 nm excitation and emission.

Virus-induced gene silencing

VIGS was performed as previously described[52]. The *UBR7* sequence was amplified and cloned into the pTRV2 vector. The constructs were transformed into *Agrobacterium tumefaciens* GV3101. *A. tumefaciens* cells were cultured in LB media containing 10 mM MES-KOH (pH 5.7), 200 μM acetosyringone, 50 mg/l gentamycin, and 50 mg/l kanamycin overnight at 28 °C, adjusted to an OD_{600} of 1.5, and infiltrated into the

first two true leaves of 2-week-old plants. After 24–26 days, VIGS plants were subjected to HS and recovery tests and gene silencing was validated using gene-specific primers (Supplementary Data 7).

Chlorophyll quantification

To determine chlorophyll content, plant leaves were ground in liquid nitrogen and immersed in 80% (v/v) acetone to extract chlorophylls. After centrifugation at 1000 × g for 15 min, the supernatant was measured at 663 and 645 nm, and chlorophyll content was calculated using the formula as previously described in ref. 86.

Sample preparation for LC-MS/MS analysis

Protein samples were prepared for proteomic analysis as previously described in ref. 87. Total proteins were extracted from plant leaves using extraction buffer (100 mM Tris-HCl, pH 7.4, 12% SDS, 20% glycerol, and 1× protease inhibitor cocktail). Proteins were incubated with 5 mM tris(2-carboxyethyl)phosphine (TCEP) (Thermo Scientific) in 50 mM ammonium bicarbonate for 30 min at 37 °C. Proteins were then transferred to YM-10 Microcon filtration devices (Millipore) and centrifuged at 14,000 × *g* for 15 min, followed by two successive washes with UA solution (8 M urea, 100 mM Tris–HCl, pH 8.5). 50 mM iodoacetamide in UA solution was added to the filter unit and incubated in the dark at room temperature for 45 min. After centrifugation at 14,000 × *g* for 15 min, proteins were washed one time with UA solution and again three times with 50 mM ammonium bicarbonate. For tryptic digestion, proteins were incubated with Trypsin Gold (Promega) using a 1:50 ratio (w/w) of trypsin to proteins overnight at 37 °C. Peptides were eluted by centrifugation at 14,000 × *g* for 15 min, followed by two centrifugations with 50 mM ammonium bicarbonate and 0.1% (v/v) formic acid. Peptides were desalted using C18 microspin columns (Harvard Apparatus) and eluted with 0.1% (v/v) formic acid in 80% acetonitrile. Peptide samples were dried under vacuum and resuspended in a solution containing 2% (v/v) acetonitrile and 0.1% (v/v) formic acid. Peptide concentrations were measured using NanoDrop (Thermo Scientific).

LC-MS/MS analysis

LC-MS/MS analysis was performed using a nanoElute LC system (Bruker Daltonics) coupled to the timsTOF Pro (Bruker Daltonics), using a CaptiveSpray nanoelectrospray ion source (Bruker Daltonics). Peptide digest (150 ng) was injected into a capillary C18 column (25 cm length, 75 μm inner diameter, 1.5 μm particle size; Bruker Daltonics). The mobile phases were 0.1% (v/v) formic acid in water (A) and 0.1% (v/v) formic acid in acetonitrile (B). Gradient elution with solvent A and B was carried out using the following settings: 120 min gradient of 2–17% B for 60 min, 17–25% B for 30 min, 25–37% B for 10 min, 37–80% B for 10 min, and 80% B for 10 min at a flow rate of 0.4 μl/min. Mass spectral data in the range of m/z 100–1700 were collected in PASEF mode[88]. Ion mobility resolution was set to 0.60–1.60 V s/cm over 100 ms ramp time, which ramped the collisional energy stepwise. Ten PASEF MS/MS scans per cycle were used for data-dependent acquisition.

Data analysis

After data acquisition, data files were processed using the Peaks Studio 10.5 software (Bioinformatics Solution) and matched to tryptic peptide fragments from the *A. thaliana* protein sequence database (UniprotKB *A. thaliana*, downloaded January 2023; 136447 entries) with up to three missed cleavages allowed[89]. The mass tolerance for precursor and fragment ions was set to 15 ppm and 0.05 Da, respectively. Variable modifications included methionine oxidation and N-terminal acetylation, and fixed modifications included carbamidomethylation of Cys residues. Significant peptide identifications were performed with false discovery rate (FDR) < 0.01.

Raw data were subjected to data preprocessing using R software. The DESeq2 package[90] was used to normalize and transform the data. Specifically, the rlog transformation was applied to normalize the data and reduce the influence of unwanted technical variation. Additionally, batch effect correction was performed using the SVA package[91] to account for any systematic differences introduced by different experimental batches. The Mfuzz package[92] was employed to cluster proteins based on their expression patterns over time. Results were visualized in R using EnhancedVolcano (RRID:SCR 018931) and pheatmap (RRID:SCR 016418).

Statistical analysis

Statistical analyses were performed using SPSS (Statistical Package for the Social Sciences). Significant differences between experimental groups were analyzed by one-way ANOVA with Tukey's HSD test or unpaired Student's *t* test for multiple or single comparisons, respectively. Detailed information about statistical analysis is provided in the figure legends. Statistical significance was set at $P < 0.05$. All experiments were repeated three to five times with similar results. For proteomics data, to compare the expression levels between groups, a moderated *t* test was performed using the limma package[93]. This test calculates log fold changes and associated *p*-values for each protein, considering the variability within and between groups. To account for multiple testing, *p*-values were adjusted using appropriate methods, such as the Benjamini-Hochberg procedure. Proteins were considered differentially expressed significantly based on the following criteria: $|\log_2 FC| \geq 1$ and $P_{adj} < 0.05$.

Reporting summary

Further information on research design is available in the Nature Portfolio Reporting Summary linked to this article.

Data availability

The mass spectrometry proteomics data have been deposited to the ProteomeXchange Consortium via the PRIDE partner repository with the dataset identifier PXD058038. Source data are provided with this paper.

References

1. Bachmair, A., Finley, D. & Varshavsky, A. In vivo half-life of a protein is a function of its amino-terminal residue. *Science* **234**, 179–186 (1986).
2. Varshavsky, A. The N-end rule pathway and regulation by proteolysis. *Protein Sci.* **20**, 1298–1345 (2011).
3. Gibbs, D. J., Bacardit, J., Bachmair, A. & Holdsworth, M. J. The eukaryotic N-end rule pathway: conserved mechanisms and diverse functions. *Trends Cell Biol.* **24**, 603–611 (2014a).
4. Holdsworth, M. J., Vicente, J., Sharma, G., Abbas, M. & Zubrycka, A. The plant N-degron pathways of ubiquitin-mediated proteolysis. *J. Integr. Plant Biol.* **62**, 70–89 (2020).
5. Hwang, C.-S., Shemorry, A. & Varshavsky, A. N-terminal acetylation of cellular proteins creates specific degradation signals. *Science* **327**, 973–977 (2010).
6. Park, S.-E. et al. Control of mammalian G protein signaling by N-terminal acetylation and the N-end rule pathway. *Science* **347**, 1249–1252 (2015).
7. Chen, S.-J., Wu, X., Wadas, B., Oh, J.-H. & Varshavsky, A. An N-end rule pathway that recognizes proline and destroys gluconeogenic enzymes. *Science* **355**, eaal3655 (2017).
8. Chen, S.-J., Kim, L., Song, H. K. & Varshavsky, A. Aminopeptidases trim Xaa-Pro proteins, initiating their degradation by the Pro/N-degron pathway. *Proc. Natl. Acad. Sci. USA* **118**, e2115430118 (2021).
9. Kim, J.-M. et al. Formyl-methionine as an N-degron of a eukaryotic N-end rule pathway. *Science* **362**, eaat0174 (2018).
10. Timms, R. T. et al. A glycine-specific N-degron pathway mediates the quality control of protein N-myristoylation. *Science* **365**, eaaw4912 (2019).

11. Sriram, S. M., Kim, B. Y. & Kwon, Y. T. The N-end rule pathway: emerging functions and molecular principles of substrate recognition. *Nat. Rev. Mol. Cell Biol.* **12**, 735–747 (2011).
12. Varshavsky, A. N-degron and C-degron pathways of protein degradation. *Proc. Natl. Acad. Sci. USA* **116**, 358–366 (2019).
13. Tasaki, T., Sriram, S. M., Park, K. S. & Kwon, Y. T. The N-end rule pathway. *Annu. Rev. Biochem.* **81**, 261–289 (2012).
14. Garzón, M. et al. PRT6/At5g02310 encodes an *Arabidopsis* ubiquitin ligase of the N-end rule pathway with arginine specificity and is not the CER3 locus. *FEBS Lett.* **581**, 3189–3196 (2007).
15. Potuschak, T. et al. PRT1 of *Arabidopsis thaliana* encodes a component of the plant N-end rule pathway. *Proc. Natl. Acad. Sci. USA* **95**, 7904–7908 (1998).
16. Kim, L., Kwon, D. H., Heo, J., Park, M. R. & Song, H. K. Use of the LC3B-fusion technique for biochemical and structural studies of proteins involved in the N-degron pathway. *J. Biol. Chem.* **295**, 2590–2600 (2020).
17. Song, H. K. et al. Structural basis for the recognition and ubiquitylation of type-2 N-degron substrate by PRT1 plant N-recognin. Preprint at https://doi.org/10.21203/rs.3.rs-5116850/v1 (2024).
18. Zhang, H. et al. BIG enhances Arg/N-degron pathway-mediated protein degradation to regulate *Arabidopsis* hypoxia responses and suberin deposition. *Plant Cell* **36**, 3177–3200 (2024).
19. Dissmeyer, N. Conditional protein function via N-degron pathway–mediated proteostasis in stress physiology. *Annu. Rev. Plant Biol.* **70**, 83–117 (2019).
20. Gibbs, D. J. et al. Homeostatic response to hypoxia is regulated by the N-end rule pathway in plants. *Nature* **479**, 415–418 (2011).
21. Gibbs, D. J. et al. Nitric oxide sensing in plants is mediated by proteolytic control of group VII ERF transcription factors. *Mol. Cell* **53**, 369–379 (2014b).
22. Licausi, F. et al. Oxygen sensing in plants is mediated by an N-end rule pathway for protein destabilization. *Nature* **479**, 419–422 (2011).
23. Chung, T. See how I eat my greens—autophagy in plant cells. *J. Plant Biol.* **54**, 339–350 (2011).
24. Marshall, R. S. & Vierstra, R. D. Autophagy: the master of bulk and selective recycling. *Annu. Rev. Plant Biol.* **69**, 173–208 (2018).
25. Zaffagnini, G. & Martens, S. Mechanisms of selective autophagy. *J. Mol. Biol.* **428**, 1714–1724 (2016).
26. Cha-Molstad, H. et al. Amino-terminal arginylation targets endoplasmic reticulum chaperone BiP for autophagy through p62 binding. *Nat. Cell Biol.* **17**, 917–929 (2015).
27. Cha-Molstad, H. et al. p62/SQSTM1/Sequestosome-1 is an N-recognin of the N-end rule pathway which modulates autophagosome biogenesis. *Nat. Commun.* **8**, 102 (2017).
28. Heo, A. J. et al. The N-terminal cysteine is a dual sensor of oxygen and oxidative stress. *Proc. Natl. Acad. Sci. USA* **118**, e2107993118 (2021).
29. Yoo, Y. D. et al. N-terminal arginylation generates a bimodal degron that modulates autophagic proteolysis. *Proc. Natl. Acad. Sci. USA* **115**, E2716–E2724 (2018).
30. Wang, P., Mugume, Y. & Bassham, D. C. New advances in autophagy in plants: regulation, selectivity and function. *Semin. Cell Dev. Biol.* **80**, 113–122 (2018).
31. Feng, Y., He, D., Yao, Z. & Klionsky, D. J. The machinery of macroautophagy. *Cell Res.* **24**, 24–41 (2014).
32. Ichimura, Y. et al. A ubiquitin-like system mediates protein lipidation. *Nature* **408**, 488–492 (2000).
33. Martens, S. & Fracchiolla, D. Activation and targeting of ATG8 protein lipidation. *Cell Discov.* **6**, 23 (2020).
34. Yoshimoto, K. et al. Processing of ATG8s, ubiquitin-like proteins, and their deconjugation by ATG4s are essential for plant autophagy. *Plant Cell* **16**, 2967–2983 (2004).
35. Bu, F., Yang, M., Guo, X., Huang, W. & Chen, L. Multiple functions of ATG8 family proteins in plant autophagy. *Front. Cell Dev. Biol.* **8**, 466 (2020).
36. Kellner, R., De la Concepcion, J. C., Maqbool, A., Kamoun, S. & Dagdas, Y. F. ATG8 expansion: a driver of selective autophagy diversification? *Trends Plant Sci.* **22**, 204–214 (2017).
37. Woo, J., Park, E. & Dinesh-Kumar, S. P. Differential processing of *Arabidopsis* ubiquitin-like Atg8 autophagy proteins by Atg4 cysteine proteases. *Proc. Natl. Acad. Sci. USA* **111**, 863–868 (2014).
38. Zou, Y. et al. ATG8 delipidation is not universally critical for autophagy in plants. *Nat. Commun.* **16**, 403 (2025).
39. Choi, W. S. et al. Structural basis for the recognition of N-end rule substrates by the UBR box of ubiquitin ligases. *Nat. Struct. Mol. Biol.* **17**, 1175–1181 (2010).
40. Latz, A. et al. TPK1, a Ca2+-regulated Arabidopsis vacuole two-pore K^+ channel is activated by 14-3-3 proteins. *Plant J.* **52**, 449–459 (2007).
41. Qi, E., Wang, D., Gao, B., Li, Y. & Li, G. Block-based characterization of protease specificity from substrate sequence profile. *BMC Bioinforma.* **18**, 1–9 (2017).
42. Gil, P. et al. BIG: a calossin-like protein required for polar auxin transport in *Arabidopsis*. *Genes Dev.* **15**, 1985–1997 (2001).
43. Adhikary, S. et al. Atypical plant homeodomain of UBR7 functions as an H2BK120Ub ligase and breast tumor suppressor. *Nat. Commun.* **10**, 1398 (2019).
44. Ivanov, A. V. et al. PHD domain-mediated E3 ligase activity directs intramolecular sumoylation of an adjacent bromodomain required for gene silencing. *Mol. Cell* **28**, 823–837 (2007).
45. Lu, Z., Xu, S., Joazeiro, C., Cobb, M. H. & Hunter, T. The PHD domain of MEKK1 acts as an E3 ubiquitin ligase and mediates ubiquitination and degradation of ERK1/2. *Mol. Cell* **9**, 945–956 (2002).
46. Amm, I., Sommer, T. & Wolf, D. H. Protein quality control and elimination of protein waste: the role of the ubiquitin-proteasome system. *Biochim. Biophys. Acta* **1843**, 182–196 (2014).
47. Borgert, L., Mishra, S. & den Brave, F. Quality control of cytoplasmic proteins inside the nucleus. *Comput. Struct. Biotechnol. J.* **20**, 4618–4625 (2022).
48. Back, S. H., Schröder, M., Lee, K., Zhang, K. & Kaufman, R. J. ER stress signaling by regulated splicing: IRE1/HAC1/XBP1. *Methods* **35**, 395–416 (2005).
49. Sedaghatmehr, M. et al. A regulatory role of autophagy for resetting the memory of heat stress in plants. *Plant Cell Environ.* **42**, 1054–1064 (2019).
50. Zhou, J. et al. NBR1-mediated selective autophagy targets insoluble ubiquitinated protein aggregates in plant stress responses. *PLoS Genet.* **9**, e1003196 (2013).
51. Burch-Smith, T. M., Schiff, M., Liu, Y. & Dinesh-Kumar, S. P. Efficient virus-induced gene silencing in *Arabidopsis*. *Plant Physiol.* **142**, 21–27 (2006).
52. Yang, Y. N. et al. The transcription factor ORA59 exhibits dual DNA binding specificity that differentially regulates ethylene-and jasmonic acid-induced genes in plant immunity. *Plant Physiol.* **187**, 2763–2784 (2021).
53. Jeon, H. S. et al. Pathogen-induced autophagy regulates monolignol transport and lignin formation in plant immunity. *Autophagy* **19**, 597–615 (2023).
54. Zhuang, X. et al. A BAR-domain protein SH3P2, which binds to phosphatidylinositol 3-phosphate and ATG8, regulates autophagosome formation in *Arabidopsis*. *Plant Cell* **25**, 4596–4615 (2013).
55. Sedaghatmehr, M. et al. Autophagy complements metalloprotease FtsH6 in degrading plastid heat shock protein HSP21 during heat stress recovery. *J. Exp. Bot.* **72**, 7498–7513 (2021).
56. Thirumalaikumar, V. P. et al. Selective autophagy regulates heat stress memory in *Arabidopsis* by NBR1-mediated targeting of HSP90. 1 and ROF1. *Autophagy* **17**, 2184–2199 (2021).

57. Espinoza-Corral, R., Herrera-Tequia, A. & Lundquist, P. K. Insights into topology and membrane interaction characteristics of plastoglobule-localized AtFBN1a and AtLOX2. *Plant Signal. Behav.* **16**, 1945213 (2021).
58. Gámez-Arjona, F. M., de la Concepción, J. C., Raynaud, S. & Mérida, Á *Arabidopsis thaliana* plastoglobule-associated fibrillin 1a interacts with fibrillin 1b in vivo. *FEBS Lett.* **588**, 2800–2804 (2014).
59. Chaudhary, S. et al. Alternative splicing and protein diversity: plants versus animals. *Front. Plant Sci.* **10**, 708 (2019).
60. Reddy, A. S., Marquez, Y., Kalyna, M. & Barta, A. Complexity of the alternative splicing landscape in plants. *Plant Cell* **25**, 3657–3683 (2013).
61. Laloum, T., Martín, G. & Duque, P. Alternative splicing control of abiotic stress responses. *Trends Plant Sci.* **23**, 140–150 (2018).
62. Ling, Y., Mahfouz, M. M. & Zhou, S. Pre-mRNA alternative splicing as a modulator for heat stress response in plants. *Trends Plant Sci.* **26**, 1153–1170 (2021).
63. Dasgupta, A., Mondal, P., Dalui, S., Das, C. & Roy, S. Molecular characterization of substrate-induced ubiquitin transfer by UBR7-PHD finger, a newly identified histone H2BK120 ubiquitin ligase. *FEBS J.* **289**, 1842–1857 (2022).
64. Zheng, Y. et al. Rice OsUBR7 modulates plant height by regulating histone H2B monoubiquitination and cell proliferation. *Plant Commun.* **3**, 100412 (2022).
65. Zhang, Y. et al. TurboID-based proximity labeling reveals that UBR7 is a regulator of N NLR immune receptor-mediated immunity. *Nat. Commun.* **10**, 3252 (2019).
66. Gibbs, D. J. et al. Oxygen-dependent proteolysis regulates the stability of angiosperm polycomb repressive complex 2 subunit VERNALIZATION 2. *Nat. Commun.* **9**, 5438 (2018).
67. Vicente, J. et al. The Cys-Arg/N-end rule pathway is a general sensor of abiotic stress in flowering plants. *Curr. Biol.* **27**, 3183–3190.e3184 (2017).
68. Brower, C. S., Piatkov, K. I. & Varshavsky, A. Neurodegeneration-associated protein fragments as short-lived substrates of the N-end rule pathway. *Mol. Cell* **50**, 161–171 (2013).
69. Chui, A. J. et al. N-terminal degradation activates the NLRP1B inflammasome. *Science* **364**, 82–85 (2019).
70. Dong, H. et al. Ubiquitylation activates a peptidase that promotes cleavage and destabilization of its activating E3 ligases and diverse growth regulatory proteins to limit cell proliferation in *Arabidopsis*. *Genes Dev.* **31**, 197–208 (2017).
71. Piatkov, K. I., Brower, C. S. & Varshavsky, A. The N-end rule pathway counteracts cell death by destroying proapoptotic protein fragments. *Proc. Natl. Acad. Sci. USA* **109**, E1839–E1847 (2012).
72. Sandstrom, A. et al. Functional degradation: a mechanism of NLRP1 inflammasome activation by diverse pathogen enzymes. *Science* **364**, eaau1330 (2019).
73. Xu, Z., Payoe, R. & Fahlman, R. P. The C-terminal proteolytic fragment of the breast cancer susceptibility type 1 protein (BRCA1) is degraded by the N-end rule pathway. *J. Biol. Chem.* **287**, 7495–7502 (2012).
74. Xu, H. et al. The N-end rule ubiquitin ligase UBR2 mediates NLRP1B inflammasome activation by anthrax lethal toxin. *EMBO J.* **38**, e101996 (2019).
75. García-Lorenzo, M., Sjödin, A., Jansson, S. & Funk, C. Protease gene families in *Populus* and *Arabidopsis*. *BMC Plant Biol.* **6**, 1–24 (2006).
76. Luo, S. et al. Cargo recognition and function of selective autophagy receptors in plants. *Int. J. Mol. Sci.* **22**, 1013 (2021).
77. Zhou, J. et al. A non-canonical role of ATG8 in Golgi recovery from heat stress in plants. *Nat. Plants* **9**, 749–765 (2023).
78. Laude, H. H. Diurnal cycle of heat resistance in plants. *Science* **89**, 556–557 (1939).
79. Dickinson, P. J. et al. Chloroplast signaling gates thermotolerance in *Arabidopsis*. *Cell Rep.* **22**, 1657–1665 (2018).
80. Bruggeman, Q. et al. Involvement of *Arabidopsis* BIG protein in cell death mediated by Myo-inositol homeostasis. *Sci. Rep.* **10**, 11268 (2020).
81. Silva-Correia, J., Freitas, S., Tavares, R. M., Lino-Neto, T. & Azevedo, H. Phenotypic analysis of the *Arabidopsis* heat stress response during germination and early seedling development. *Plant Methods* **10**, 1–11 (2014).
82. Kwon, D. H. et al. The 1: 2 complex between RavZ and LC3 reveals a mechanism for deconjugation of LC3 on the phagophore membrane. *Autophagy* **13**, 70–81 (2017).
83. Wang, W., Liu, N., Gao, C., Rui, L. & Tang, D. The *Pseudomonas syringae* effector AvrPtoB associates with and ubiquitinates *Arabidopsis* exocyst subunit EXO70B1. *Front. Plant Sci.* **10**, 1027 (2019).
84. Walter, M. et al. Visualization of protein interactions in living plant cells using bimolecular fluorescence complementation. *Plant J.* **40**, 428–438 (2004).
85. Kwon, S. I., Cho, H. J., Kim, S. R. & Park, O. K. The Rab GTPase RabG3b positively regulates autophagy and immunity-associated hypersensitive cell death in *Arabidopsis*. *Plant Physiol.* **161**, 1722–1736 (2013).
86. Lichtenthaler, H. K. Chlorophylls and carotenoids: pigments of photosynthetic membranes. *Methods Enzymol.* **148**, 350–383 (1987).
87. Wiśniewski, J. R., Zougman, A., Nagaraj, N. & Mann, M. Universal sample preparation method for proteome analysis. *Nat. Methods* **6**, 359–362 (2009).
88. Meier, F. et al. Parallel accumulation–serial fragmentation (PASEF): multiplying sequencing speed and sensitivity by synchronized scans in a trapped ion mobility device. *J. Proteome Res.* **14**, 5378–5387 (2015).
89. Zhang, J. et al. PEAKS DB: de novo sequencing assisted database search for sensitive and accurate peptide identification. *Mol. Cell Proteom.* **11**, M111010587 (2012).
90. Love, M. I., Huber, W. & Anders, S. Moderated estimation of fold change and dispersion for RNA-seq data with DESeq2. *Genome Biol.* **15**, 1–21 (2014).
91. Leek, J. T., Johnson, W. E., Parker, H. S., Jaffe, A. E. & Storey, J. D. The sva package for removing batch effects and other unwanted variation in high-throughput experiments. *Bioinformatics* **28**, 882–883 (2012).
92. Kumar, L. & Futschik, M. E. Mfuzz: a software package for soft clustering of microarray data. *Bioinformation* **2**, 5 (2007).
93. Ritchie, M. E. et al. limma powers differential expression analyses for RNA-sequencing and microarray studies. *Nucleic Acids Res.* **43**, e47 (2015).

Acknowledgements

We thank Liwen Jiang for sharing SH3P2-GFP seeds. This work was supported by a Korea University grant and National Research Foundation of Korea (NRF) grants (RS-2024-00339452, RS-2025-00512558) from the Korean government (MSIP) to O.K.P.

Author contributions

O.K.P. conceived and directed the project. S.H.K. and O.K.P. designed the research. S.H.K. performed most of the experiments. J.S.P., M.H.L. and J.P. participated in immunoblotting and RT-qPCR analysis. J.S., J.K., K.Y., J.C. and J.B.S. conducted proteomics analysis. W.S.Y. and H.K.S. performed protein purification. S.H.K. and O.K.P. analyzed the data and wrote the manuscript. All authors contributed to the review and editing of the manuscript.

Competing interests

The authors declare no competing interests.

Additional information

Supplementary information The online version contains supplementary material available at https://doi.org/10.1038/s41467-025-61191-5.

Correspondence and requests for materials should be addressed to Ohkmae K. Park.

Peer review information *Nature Communications* thanks Kohki ?Yoshimoto, who co-reviewed with Keisuke Seta, Markus Wirtz, and the other anonymous reviewer(s) for their contribution to the peer review of this work. A peer review file is available.